Simulation of a Wind Powered Freshwater and Electricity Production System

Numerical Modeling and Optimization

A.I. Goveas

DOT

TU Delft

Simulation of a Wind Powered Freshwater and Electricity Production System

Numerical Modeling and Optimization

MASTER OF SCIENCE THESIS

by

A . I. Goveas

For the degree of Master of Science in Sustainable Energy Technology at Delft University of Technology

August 21, 2020

Faculty of Electrical Engineering, Mathematics and Computer Science (EEMCS)

Abstract

The rapid growth in world population and increasing demands have led to the lack of fresh water, taking a toll on several of earths reserves, mainly the fresh water supply reserves. Water stress deters economic growth, leads to conflicts and has a direct impact on the health of humans. Studies show the trends in the increase of water consumption per capita due to increase in higher standards of living over the last years, resulting in the decrease of usable high purity water. 97% of the world's water supply is locked in the salted, often unusable oceans. In recent times, water stressed countries are using the saline water from the oceans and desalinating it to produce fresh water for domestic, industrial or agricultural use. The state-of-the art method for desalinating saltwater is by Reverse Osmosis (RO). The biggest drawback of this technology is its high energy consumption mostly provided by conventional sources like fossil fuels. Therefore, for a sustainable future, a renewable energy source must be integrated to power the RO system.

Delft Offshore Turbine (DOT) is currently developing and testing a new hydraulic drive train solution for fluid power transmission in offshore wind turbines using seawater as the medium. A hydraulic positive displacement pump is driven by the DOT wind turbine creating a flow of sea water under high pressure. This high-pressure flow can be either directed to a RO unit to desalinate seawater or converted into electricity using a spear valve and pelton turbine generator. A major challenge while using wind as an energy source is its intermittency. Reverse osmosis plants are designed to operate at a fixed flow and pressure while due to the uncontrolled, varying nature of the wind, the pump output experiences fluctuations in both pressures and flows.

The aim of this thesis is to analyze the steady-state behavior of the integrated system for wind speeds up to the turbine rated wind speed under different operating conditions. This is achieved by simulating the behavior of the DOT500 hydraulic drive train wind turbine coupled to a RO system with pressure exchanger energy recovery device and a nozzle with a pelton turbine generator. The main objective of this research is to build a numerical model in Python using algorithms to solve the system of steady-state equations and optimize the integrated system for maximum water and maximum electricity production at specified locations.

The numerical model is simulated for all combinations of wind speeds and nozzle positions and the behavior of the high-pressure pump, RO system, pelton turbine and various system parameters are shown. A sensitivity study is performed for important desalination parameters and their effect on system performance is analyzed.

This research has yielded three main conclusions / deliverables:

1. Behavior of the wind powered integrated system to produce freshwater and electricity at different operating conditions.
2. Steady state control of DOT500 turbine and behavior of the pelton turbine to produce either maximum electricity or maximum water.
3. Sensitivity of important desalination system parameters on overall system behavior for future optimization of RO membranes.

Acknowledgements

My journey at the Delft University of Technology has been unreal. I have enjoyed and cherished every bit of this unbelievable journey. This thesis concludes my academic career at TU Delft and is a result of hard work and determination. Everything that I have experienced in life previously, every little decision that I made, has led to this moment and I am nothing but grateful for this opportunity.

Firstly, I would like to express my gratitude towards my supervisor at the university, Dr. ir. Michiel Zaayer. I look up to you and your scientific knowledge and someday I aspire to think critically like you. Without you and your constant support, this wouldn't have been possible. A special thanks to Dr. Dominic von Terzi for presiding over the chair of my graduation committee.

I also want to thank Dr. Niels Diepeveen for giving me this opportunity to graduate on such an interesting project at DOT. Your vision and work in this field will change the way we tackle water shortage problems, especially in coastal developing countries. Coming from a coastal city in India, with water shortages every summer, this is nothing short of a technological revolution.

I would like to express my sincere gratitude and deepest appreciation to my daily supervisor Ms. Francesca Greco for the continuous support and assistance, feedback and guidance and the discussions during weekly meetings. A special thanks goes out to Deborah, Alejandro and everybody at DOT for the very pleasant environment.

Last, but not the least, I express my sincere gratitude to my Mum, Dad and brother for the unconditional love and endless support both morally and financially for the entire length of my academic journey. I would never have enjoyed these opportunities without you. My sincere thanks to the Louis family for the constant emotional support. Thank you for giving me the strength to reach for the stars and chase my dreams.

To my ever-loving girlfriend, Kavya, thank you for everything. You stood by me through thick and thin.

To 9x, you guys are my source of entertainment. To Daniel, Rohit, Saumitra, Alexandros, Sahil and all my friends here in Europe and back in India, Thank you from the bottom of my heart.

Table of Contents

Nomenclature

Symbols and Abbreviations

α	Cone angle of spear
Δ	Difference
$\Delta\Pi$	Osmotic Pressure Difference
γ	Recovery ratio
λ	Tip speed ratio
η	Efficiency
ω	Rotational speed
ρ	Density
τ	Torque
A	Area, Weibull Scale parameter
A_m	Membrane active area
A_{nz}	Effective nozzle area
C	Concentration, Coefficient
C_d	Coefficient of Discharge
C_{eff}	Effective concentrate at RO membrane surface
C_p	Power Coefficient
C_c	Torque Coefficient
D_{nz}	Spear valve nozzle Diameter
DOT	Delft Offshore Turbine
DOT500	500 kW Delft Offshore Turbine
E	Energy
ERD	Energy Recovery Device
G	Gearbox ratio
HPP	High-Pressure Pump
J	Flux, Mass moment of Inertia
k	Weibull Shape parameter

K	constant
K_{opt}	Turbine maximum power control curve
K_w	Permeability constant
L	Leakage
n	number of
nz	nozzle
OF	Over Flush
p	Pressure
P	Power
PX	Pressure exchanger
Q	Flowrate
R	Radius, Salt rejection, Boltzmann constant
RO	Reverse Osmosis
s	Nozzle Displacement
SP	Salt Passage
SWRO	Sea water Reverse Osmosis
T	Temperature
t	Time
U	Wind speed
V	Volumetric displacement
VM	Volumetric Mixing

List of Figures

List of Tables

Chapter 1: Introduction

The purpose of this chapter is to introduce the problem which this thesis will try to solve. Background information of the problem is stated, followed by the problem definition. Finally, the objective of this thesis, methodology used to tackle it and the structure of this thesis will be described.

1.1 Background on water desalination

The higher standards of living and the significant increase in the world's population has resulted in the increase of per capita water consumption over the last years and has, thus, led to a decrease of high purity usable water. The trends show that the natural freshwater resources are severely exploited and, in most cases, depleted making it necessary to pursue alternative freshwater resources. Nearly 70% of the earth is covered by water, of which only 2.5% is fresh water [1]. Glaciers and permanent snow constitute most of this fresh water. Table 1.1 shows the global water mix indicating that most water is oceanic water, which when treated can be used as fresh water for drinking, agricultural or industrial purposes. The dissolved salts are removed by desalination, thus providing a way of converting this sea water or brackish groundwater into fresh water. Sustainable ways of producing freshwater are vital to supply the need as the demand for fresh water grows at an exponential rate.

Table 1. 1: Global water stock [1]. Adapted from [2].

Location	Volume (*10^6 km^3)	Percentage (%)
Oceans	1338.0	96.54
Ice caps, Glaciers & Permanent snow	24.06	1.74
Groundwater (Brackish or saline)	12.87	0.93
Groundwater (Fresh)	10.53	0.76
Ground Ice & Permafrost	0.30	0.022
Lakes (Fresh & Saline)	0.176	0.013
Rivers	0.002	0.0002
Atmosphere, Swamps & Biological water	0.025	0.0019
Atmosphere	0.012	0.001

Production of water through desalination is increasing globally over the last few years. According to the International Desalination Association water security handbook, 2019 – 2020 [3], the number of desalination plants have increased from 1,500 in 2012 to 21,123 in 2020. The total cumulative desalination capacity in 150 countries is 126.57 million m^3/day out of which 63% is generated out of sea water feed (i.e. oceans) and 19% originates from brackish water sources [3]. More than 300 million people around the world rely on desalinated water for all their daily needs [3]. This is mainly because of the rapid population & economic growth, major changes in lifestyle, and extreme scarcity of renewable freshwater resources.

The desalination plants in Europe are concentrated around the Mediterranean Sea due to water shortages and sea water abundance in these regions. Concerns about the negative impact on the environment of operating these plants are raised due to the rapid increase in the construction of desalination plants worldwide. The biggest drawback of desalination is its high energy consumption compared to other technologies like filtration, sedimentation and distillation. Currently, most of these plants are operated

using electricity generated by fossil fuels as the main energy source, thus emitting air pollutants like greenhouse gases. Therefore, these have a large impact on climate change.

Theoretically, the absolute minimum amount of energy needed to desalinate seawater is 1 kilowatt-hour per cubic meter of usable water produced or 3.5 kilowatt-hours per thousand gallons (kWh/kgal) [4]. According to Akgul et al. [6] , around 70% of the costs to operate saltwater reverse osmosis is the cost of electricity. Hence the prices of electricity play the deciding factor for the cost of fresh water. Most of the desalination plants currently run on electricity generated from fossil fuels taking into account the low fuel costs, especially in middle eastern countries. For every cubic meter of fresh water produced from the current state-of-the-art Reverse Osmosis (RO) desalination plants, emission is between 1.2 and 1.5 kg of CO_2 [7].

This has led to a significant increase in the research for using alternative energy sources as the primary input for desalination processes, like solar or wind power. A report by Bloomberg [8] shows that the majority of countries facing water shortage, currently and in the future, have a large amount of renewable energy sources. These countries are mainly in Africa, the gulf region and in Asia.

The wind farms being built currently with hundreds of megawatts in capacity have the potential to produce huge amounts of water at an economical cost. The power output from a wind turbine is dynamic at wind speeds lower than the rated wind speed. This intermittency of wind poses a major drawback to coupling these technologies with desalination. Another drawback is that these technologies are first used to convert energy into electrical energy and this electricity is used to power desalination processes. Thus, losses of energy are induced due to transmission and conversion which leads to lower efficiencies.

Reverse osmosis is an energy intensive process, mainly because of the need for high pressures at the inlet. The energy can be recovered from the concentrate (high salt concentration) stream which exits the RO unit at inlet pressures by using Energy Recovery Devices (ERDs), thus making the desalination processes more efficient.

1.2 Water desalination with the Delft Offshore Turbine

Delft Offshore Turbine (DOT) was established in 2008 as a project set up by DUWIND, an energy research branch of the Delft Institute of Technology. The main idea of the project was to make offshore wind energy a competitive energy source without subsidies. The approach was to redesign and restructure the way energy from the wind is integrated to different processes like desalination or transported back to the grid. Niels Diepeveen [5] proposed a way to apply fluid power transmission in large offshore wind turbine drive trains. This wind turbine drives a hydraulic pump directly to feed high pressure feed water for desalination, rather than using the intermediate step of electricity generation.

A combination of the DOT turbine with a RO system coupled to an ERD was analyzed in more detail by Roy Smith [9] by designing and constructing a downscaled experimental setup and validating the experimental results using a numerical model. Furthermore, the behavior of the RO system under variable conditions has been studied in detail by MF Supper [10] to investigate the effect of fluctuating pressures and flows on permeate production. When DOT is used to desalinate seawater via RO, the residual energy that is available, but unused, can be used to drive a pelton turbine and generate electricity.

1.3 Problem definition

The integration of a hydraulic drive train wind turbine system together with a reverse osmosis system to desalinate sea / brackish water and a pelton turbine to generate electricity has only been done in literature. The DOT system technology is in its research and development phase of the learning curve. Although, detailed study and system modeling has been made to integrate the DOT separately with a RO

system and a pelton turbine, a study on combination of both RO and pelton turbine with an ERD has not been done. The behavior of the RO system under varying conditions is also known precisely. Moreover, there is insufficient knowledge in optimizing the integrated system for either maximum water / electricity production using only a nozzle. Simulating the wind powered freshwater and electricity production system can help in gaining in depth knowledge of the behavior of various integrated system components and processes at different wind speed conditions. This results in a better understanding of the influence of the intermittency of the nature of wind on system performance and turbine operation. Depending on the location of installation of the system, optimization can be done using the simulation to either produce maximum water or maximum electricity or a favorable combination of the both with the end goal of maximizing revenue from system operation. An insight into the use of spear valve as a control mechanism on the performance of a wind driven desalination system is determined to lay a basis for future research on its exact influence on system stability.

1.4 Thesis Objective

This thesis focuses on the production of fresh water using a RO system coupled to an energy recovery device and electricity using a pelton turbine integrated to a 500 kW DOT hydraulic drive train wind turbine (DOT500). The main aim of this research is to investigate the steady-state behavior of the integrated system using a spear valve and optimize the system for maximum electricity/water production. In particular, the influence of the spear valve on the control of the wind turbine, systems' pressures and flows and behavior of the pelton turbine is analyzed.

This translates to the main research question:

How can the DOT500 hydraulic drive train wind turbine be used to produce fresh water and electricity using a spear valve as means to control and optimize the system?

The goal of this research is to quantitatively learn and understand the performance of various system parameters under different operating conditions. For this, the several sub-objectives are stated below:

1. *Having a numerical model that solves the system for all combinations of operating conditions to help in better understanding of the system behavior.*
2. *Performing case studies of simulations and optimization for maximum water and electricity production to help obtain the stable operation of the DOT500 turbine.*
3. *Sensitivity analysis of critical desalination parameters on overall system behavior to obtain guidelines for operating the DOT/RO system.*

1.5 Methodology

The main purpose of this research is to simulate the system shown in Figure 1.1 below. A generic numerical model is constructed for combining the DOT500 with a pelton turbine for electricity generation and a reverse osmosis system coupled to a pressure exchanger energy recovery device for water production.

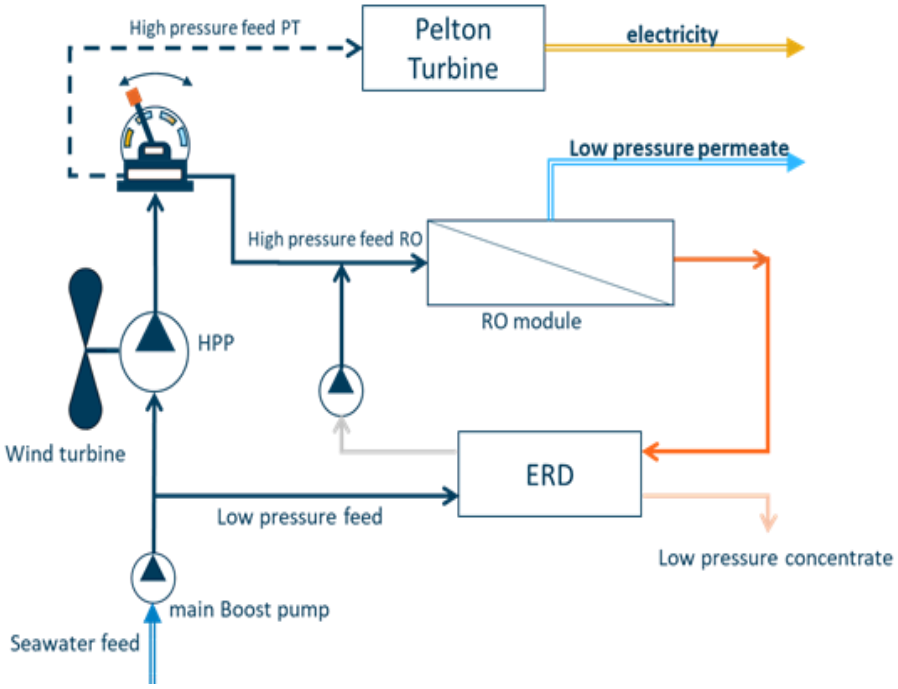

Figure 1. 1 General overview of the DOT system.

The system is solved using an algorithm written in Python. A spear valve is used as the main control mechanism for the system operation. The behavior of various system parameters are presented for up to rated wind speeds and all positions of the nozzle in the spear valve, to understand the system behavior under different operating conditions. The system parameters include the system operating pressure, flow rates from the high-pressure pump to both the pelton turbine through the nozzle and RO unit through the valve and torque and rotational speeds of the DOT500 turbine and pelton generator.

Optimization of the designed system is performed for maximum water production and maximum electricity production with an objective to maximize the revenue generated for three locations namely Maasvlakte in The Netherlands, Aruba South and Aruba North in the southern Caribbean Sea. The steady state set points for both cases of optimization using the nozzle along with the behavior of various system components and turbine operating curves are presented.

Finally, sensitivity analysis is performed for important system parameters like the permeability coefficient, K_w and active area of the membrane, A_m, and the results are analyzed.

1.6 Report Structure

The structure of this report is described here. In Chapter 2, first the fundamentals of reverse osmosis are explained briefly with a schematic overview of a basic RO membrane system. Then, the working principle of a Class I pressure exchanger energy recovery device used in the system is presented. A detailed description on the DOT concept wind turbine, hydraulic drive train and the spear valve is followed to give the reader an overview of the system. The design of the numerical model of wind powered freshwater production system is shown in Chapter 3 with the governing equations and schematic representations of system parameters. The algorithm used to solve the system of equations governing the model design is explained in detail. A description of the numerical model for the operation of the RO system, boost pump and pelton turbine is further discussed followed by the model for power consumption of the system. The

simulations for various scenarios, using the numerical model built, are performed in Chapter 4. First, the model is simulated for operating the wind turbine at maximum power performance and the results are presented. This is followed by simulation of the system for all wind speeds and nozzle positions within the range of operation using the algorithm described in Chapter 3. Optimization of the system for maximum electricity production and maximum water production for three locations namely Maasvlakte in the Netherlands, Aruba north and Aruba south, is performed using separate algorithms and the corresponding results are presented and analyzed in Chapter 5. In Chapter 6, sensitivity analysis of important desalination parameters is performed and their effect on system performance is analyzed. Finally, conclusions and recommendations for future research are drawn in Chapter 7.

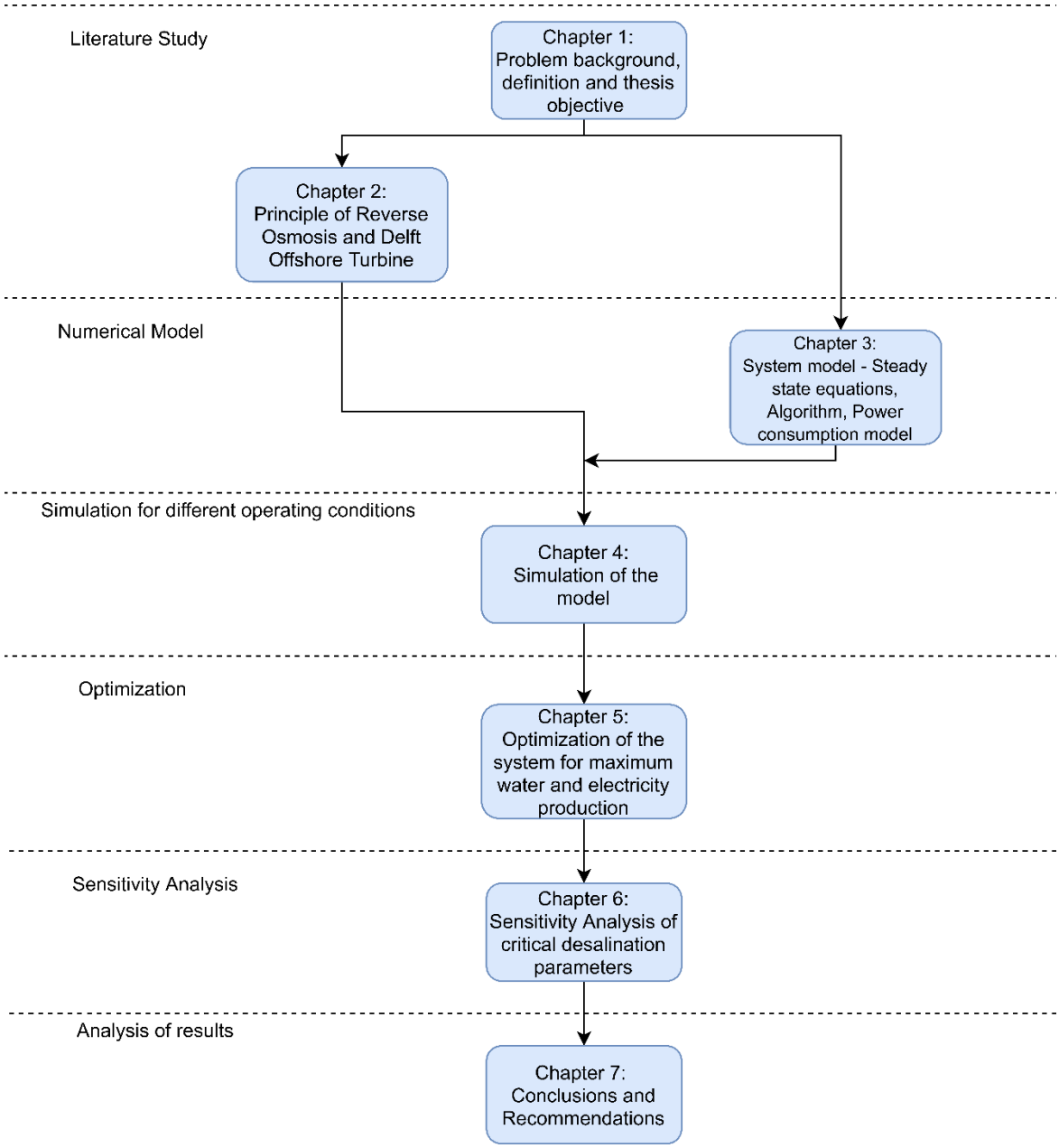

Figure 1. 2 Thesis report structure.

Chapter 2: Principle of Reverse Osmosis and DOT concept Turbine

The purpose of this chapter is to provide information about the fundamentals of reverse osmosis and the energy recovery device. The working principles of DOT concept hydraulic drive train wind turbine are discussed in this chapter. If the reader is already familiar with these topics, Chapter 2, or parts of it can be skipped.

2.1 Fundamentals of RO:

Reverse osmosis is a membrane-based separation technique based on a semi-permeable membrane where the solvent or water can pass through the membrane but dissolved matters, such as salts or dissolved organic matter, are retained.

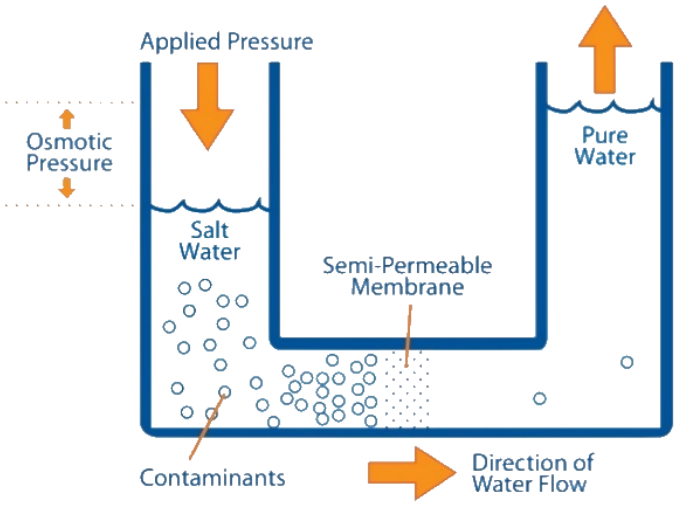

Figure 2. 1 Principle of Reverse Osmosis.

A general schematic overview of the RO membrane separation process is shown in Figure 2.2 below.

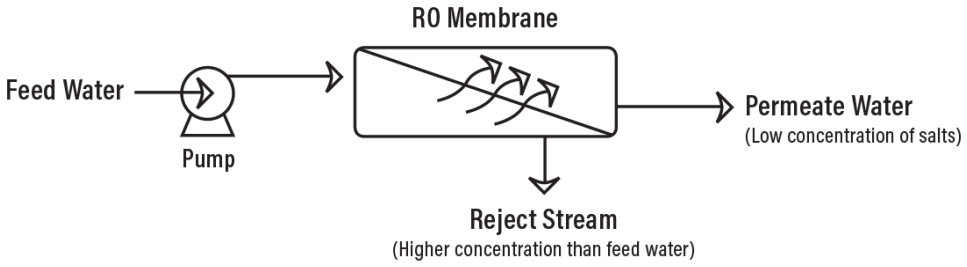

Figure 2. 2 Schematic showing the configuration of the RO membrane system [11].

Reverse osmosis occurs when a fairly high pressure is applied to the inlet feed flow (sea/brackish water) to overcome the so called 'osmotic pressure'. Typical values for the osmotic pressure, ΔΠ, for seawater having the concentration of salts between 28000-35000 ppm lie around 25 to 35 bars. For pressures higher than the osmotic pressure, water is desalinated. Typical RO plants operate in the range from 65 to 80 bar feed pressures to optimally desalinate seawater. Most of the RO desalination plants utilize the cross-flow technique using spiral wound membranes to avoid fouling at the membrane surface. This technique creates sufficient turbulence in the flow to sweep away buildup of contaminants, thus keeping the membrane surface clear.

The stream of feed seawater at high pressures flow through the semi-permeable membrane used in the RO process. The membrane blocks the passage of most of the dissolved salts, bacteria, algies, suspended solids, organic macro molecules and pyrogens and only allows fresh water to flow through it [11]. Dissolved ions like Na^+ and Cl^- are rejected by the RO polymer filter whose pore sizes are smaller than 1 nanometer [11].

Raw feed water from the sea is pumped using a high-pressure hydraulic pump as feed onto the membrane surface. If the pressure of the feed stream is above osmotic pressure, the RO module splits it into two streams. The permeate (fresh) stream at a low atmospheric pressure and the concentrate (reject) stream at a higher pressure, close to feed pressure. The concentrate stream can be fed to either another stage of desalination in order to further recover the permeate or as an input to an Isobaric Pressure Exchanger (PX) ERD to recover the pressure energy.

Two driving forces are responsible for the transport through membranes: diffusion and pore flow. To which extent one of the two driving forces is dominant depends on the membrane pore diameter [10]. For filtration techniques using membranes with larger pore diameter such as ultrafiltration and microfiltration, pore flow transport is dominant. For nanofiltration, a combination of both diffusion and pore flow play an important role in the transport of fluid medium through the membrane [26]. Transport through reverse osmosis membranes is purely controlled by diffusion. This is mainly because of the lack of open channels which could provide pore flow [12][13].

The transport of solution through the membrane for RO consists of 3 steps [14]:

(i) Absorption of feed onto the membrane surface

(ii) Diffusion through the membrane thickness

(iii) Desorption from the permeate-side surface of the membrane.

The Recovery ratio, of a RO membrane is defined as the ratio of permeate flow rate divided by feed flow rate. It is the percent of feedwater which becomes fresh water and varies between 35% and 85% [9]. Recovery ratio depends on various factors like type of pre-treatment , temperature, salinity and composition of feed water, system operating pressure and disposal of concentrate depending on the location of the plant [15]. The performance of the RO membranes depends on mainly the type of its configuration inside the pressure vessels: plate and frame configuration, hollow fiber configuration and spiral wound configuration. Spiral wound configuration is the most efficient and cost effective. For seawater reverse osmosis (SWRO), 30% to 50% of permeate water can be extracted from the feed water [21]. The concentrate stream usually has around 98% to 99.8% of dissolved salts in it depending on the salt rejection rate of the membrane. The salt rejection rate, R, indicates the quantity of salt rejected from the feedwater stream by the RO membrane as a percentage. The term salt passage also describes the quantity of salt which passes through the RO membrane into the permeate stream.

A study by Roy Smith [9] on the percentage of NaCl salt molecules passing through a membrane at different concentration shows that for feed water at very low salinities, below 200 mg/L, the salt passage is high. This causes the permeate stream to be saline. For feed water salinities between 200 mg/L and 400 mg/L, the salt passage decreases rapidly. Between 400 mg/L and 1500 mg/L of salinity in feed water, the salt passage increases gradually again [9].

A Class I isobaric pressure exchanger (PX) energy recovery device named iSave, designed by Danfoss is coupled in parallel to the RO system as shown in Figure 2.3 below. The class I ERD's convert the hydraulic pressure energy from the outlet concentrate stream directly into hydraulic energy.

In Reverse osmosis, the fresh water permeate is collected at near atmospheric pressure. The concentrate brine stream exits the RO unit at high pressure (near inlet feed pressure) because the only loss in energy is due to turbulence of the flow through the porous spacers [9]. This concentrate brine contains a large fraction of the inlet pressure energy that can be recycled using an ERD. ERDs can make the reverse osmosis systems substantially more efficient by redirecting the pressure recovered back to the feed high-pressure pump. More than two thirds of the total cost in operating RO plants is the cost of energy consumption. Currently, the energy requirement of state of the art SWRO plants is as low as 1.6 kWh/m^3 [16]. This is because ERDs can reduce the specific energy consumption between 2-3 kWh/m^3 [16].

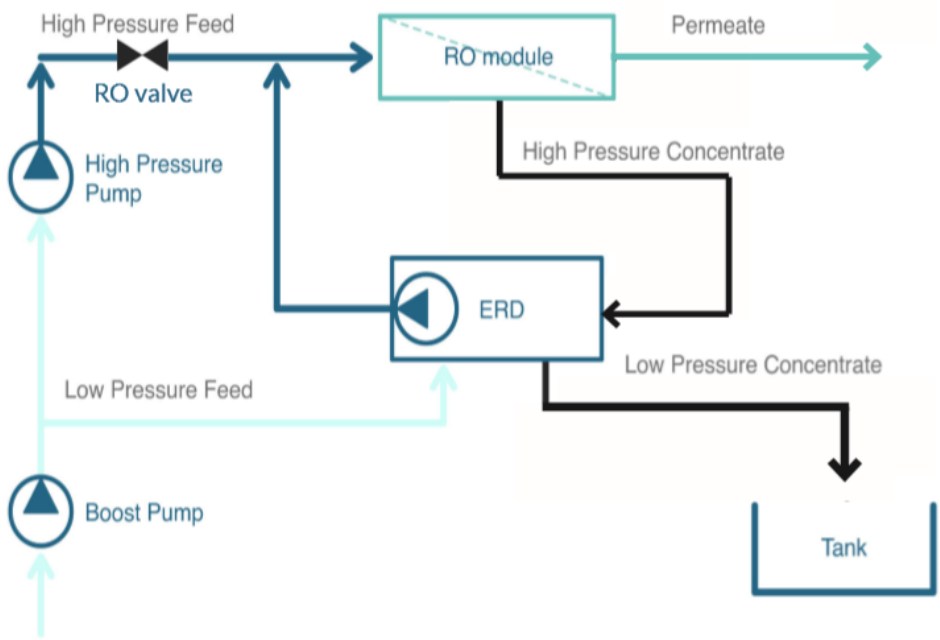

Figure 2. 3 Principle of Class I pressure exchanger energy recovery system.

The working principle of a Class I iSave ERD is explained below using Figure 2.4 [9]:

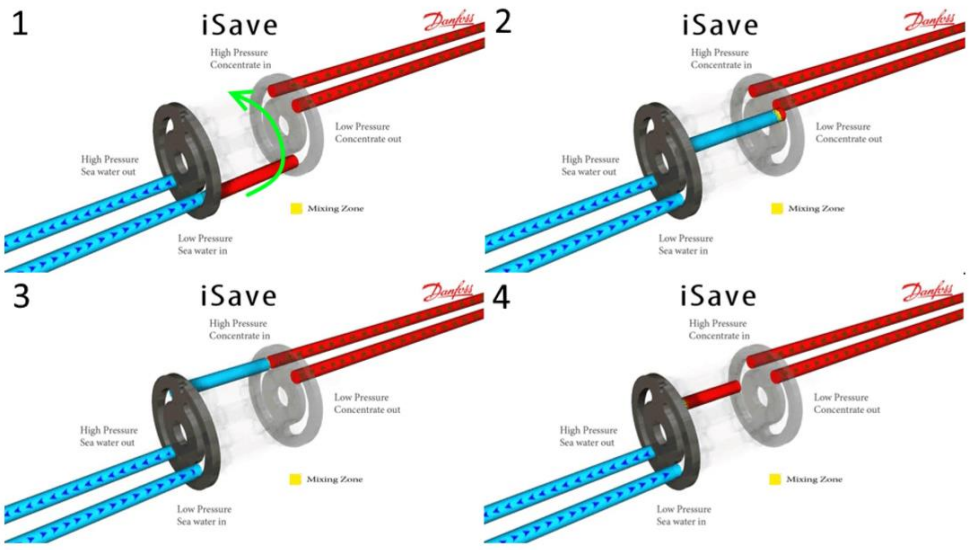

Figure 2. 4 Working principle of an isobaric iSave ERD [17].

The central part in Figure 2.4-1 represented by the grey cylinder is the rotor. The rotor rotates with the help of an electric motor in the direction as indicated by the green arrow. The rotor consists of several chambers which aid in energy transfer between high-pressure and low-pressure fluids through continuously rotating chambers [28]. The rotational speed of the rotor depends on the flow rate of the concentrate stream. The boost pump (sea water pump) provides the feed sea water at low pressure into the rotor as seen at 1. This causes the low-pressure concentrate reject that was present in the chamber to drain. The rotation of the rotor causes the chamber to be filled completely with low-pressure feed sea water as seen at 2. The hydraulic energy of the high-pressure concentrate stream is transferred to the feed water at 3. This converts the low-pressure feed stream to a high-pressure feed stream to be fed into the RO membranes. The feed water is now pushed out of the chamber at 4 and the chamber contains low pressure brine water and thus the cycle repeats. The efficiency of the PX ERD remains constant at all the flow rates within its operating range [16].

2.2 Delft Offshore Turbine (DOT)

Delft Offshore Turbine B.V. (DOT B.V.) is a private company under De Oude Bibliotheek (DOB-Academy). The main focus of the company is the development of hydraulic drive train for offshore wind development. The DOT500 is a redesign of a Vestas V44 where the drive train has been replaced by a hydraulic transmission line. Fluid transmission is already a mature technology and has been used to transport energy in multiple sectors. A schematic overview of the DOT turbine principle is shown in Figure 2.5 below.

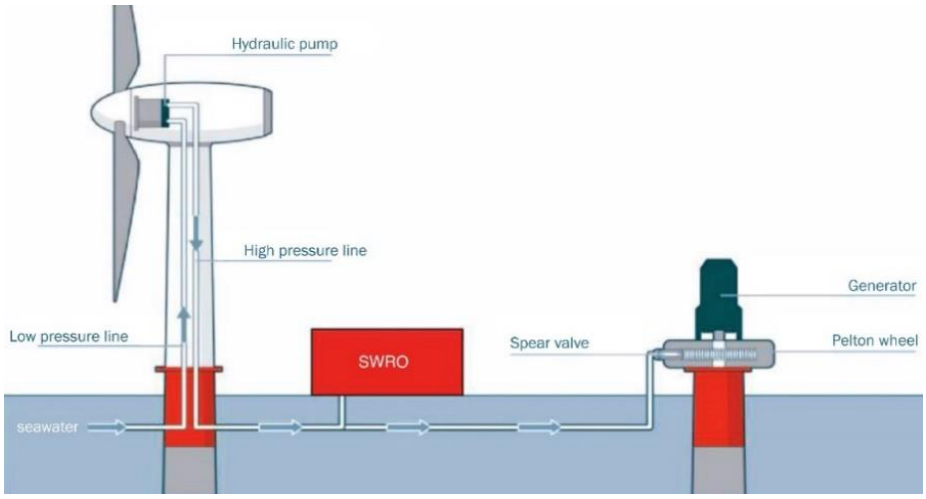

Figure 2. 5 A schematic overview of DOT500 wind driven Reverse osmosis system with a Pelton turbine.

The turbine has a rated power of 500kW and a rotor diameter of 44 meters. The coefficient of power, C_p and coefficient of torque, C_c of the DOT500 hydraulic drive train wind turbine are plotted in Figure 2.6 as a function of tip speed ratio.

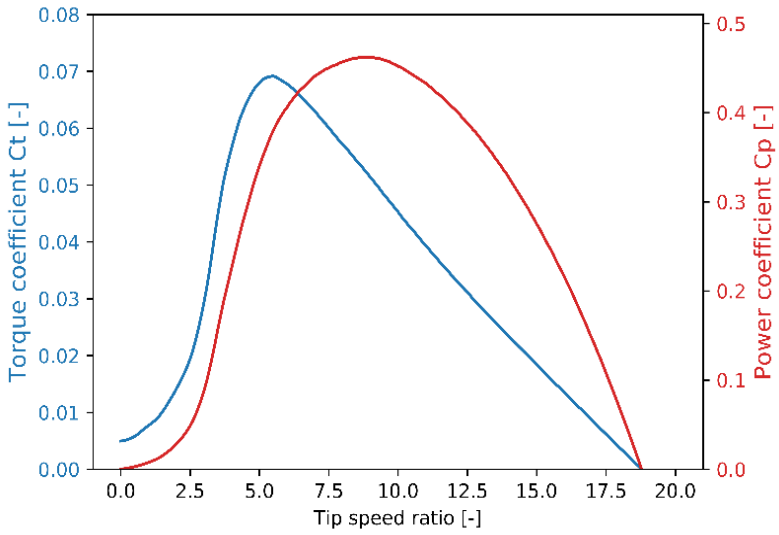

Figure 2. 6 $C_p - \lambda$ (red) and C_c - λ (blue) curve of DOT500.

The tip speed ratio, λ is defined as the ratio between the speed at the blade tip and the incoming wind speed. These curves determine the performance of the rotor. As seen in Figure 2.6, at a tip speed ratio of 0, the rotor does not rotate and hence no power is extracted from the wind. Therefore, C_p becomes 0. At a tip speed ratio of 18.75, the blades spin too fast and hence the blurring blades appear like a solid wall to the wind. The blades spin through turbulent wind and hence there is no mass transport through the rotor. Thus, no energy is extracted from the moving wind and C_p becomes 0. The maximum coefficient of torque, $C_{c,max}$ is 0.0692 at a tip speed ratio of 5.5. The maximum power is extracted at the optimal tip speed ratio, λ_{opt} equal to 8.6 and the corresponding value for coefficient of power, $C_{p,max}$ is 0.462.

A schematic overview of the DOT concept hydraulic drive train wind turbine in combination with a reverse osmosis unit coupled to an ERD and a pelton turbine with a spear valve as a nozzle is shown in figure 2.7 below:

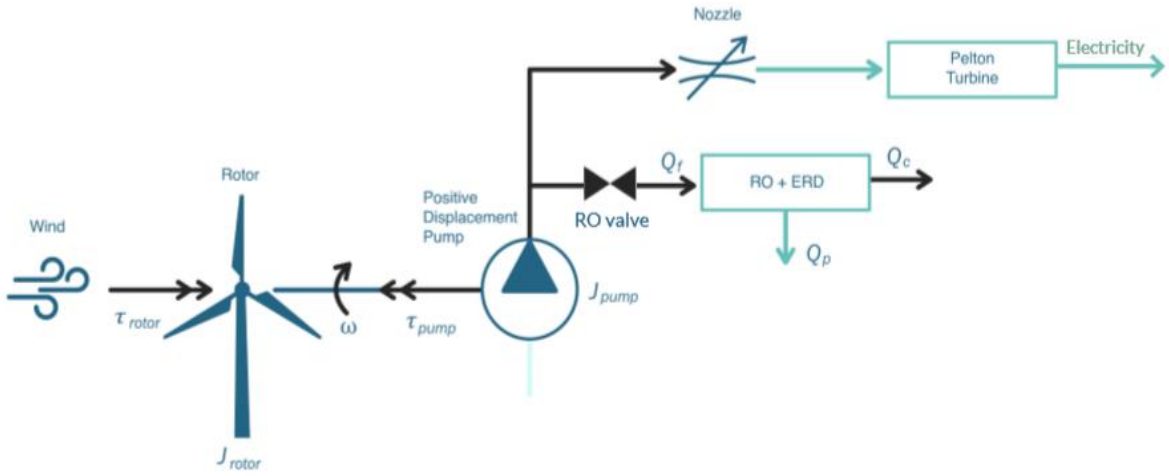

Figure 2. 7 Overview of a hydraulic drive train coupled to RO & nozzle.

A hydraulic drive train wind turbine consists of a positive displacement pump in the nacelle, replacing the traditional generator. The main control principle of such a drive train is to control the speed of the rotor to extract power from the wind as efficiently as possible. The wind speed is an environmental parameter, has high temporal variation and cannot be influenced. It determines the torque on the rotor. Hence, the rotational speed of the rotor shaft is also varying if no adaptive counter torque is produced. However, the rotor rotational speed can be regulated below rated wind speeds by applying a counter torque. The hydraulic pump acts as a counter torque to control the wind turbine by controlling the pressure in the high-pressure line via opening and closing of the spear valve. The spear valve works as a resistance. Thus, the torque of the pump can be controlled. The hydraulic energy produced by the positive displacement pump can be converted back into mechanical energy using a pelton turbine. A generator can be coupled to a pelton turbine to convert this mechanical energy into electrical power. In addition, a valve is used between the high-pressure pump and the RO module in order to switch the flow to the RO module on and off.

The spear valve used as a nozzle in the DOT system is depicted in figure 2.8 below:

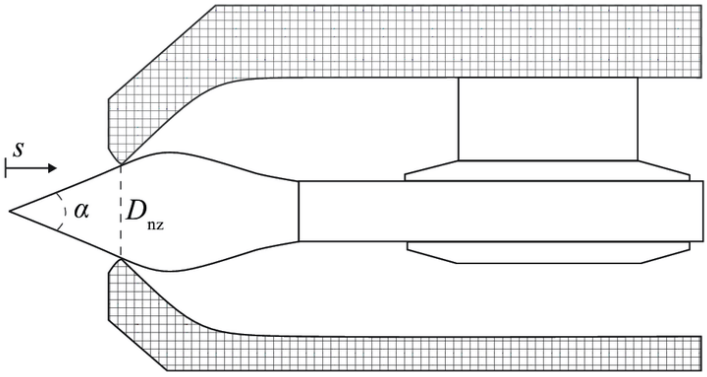

Figure 2. 8 Schematic representation of the cross section of a spear valve [19] .

where α is the coning angle of the spear which is 50̊, D_{nz} is the diameter of the nozzle, that is 38 mm, and s is the position of the tip of the spear in the nozzle. The effective outlet area of the nozzle A_{nz} is adjustable by the nozzle position s.

The combination of using a RO unit for desalination and a pelton turbine via a spear valve to generate electricity will be the focus of this thesis. The spear valve thus can be used to both produce electricity, by impinging the high-pressure flow via a valve on a pelton turbine, and as a means to control the turbine rotational speed and the pressure in the pipeline to the RO module.

Chapter 3: Numerical model of DOT system

In this Chapter, the numerical model of a wind powered SWRO desalination system is designed based on the components used in Figure 1.1. For the transmission system in the nacelle, the low speed shaft of the DOT500 rotor connects to a gearbox with a reduction factor, G of 52.5. The high-speed shaft coming out on the other side of the gearbox is connected to the Kamat Pump. The pump has a volumetric displacement of 1.61 [L/rev.]. The pump has a volumetric efficiency of 93% and a mechanical efficiency of 90%.

The Kamat high-pressure pump (HPP) is connected to a RO unit consisting of 6 pressure vessels with 6 membranes each, on one side, and to a pelton turbine generator via a spear valve on the other side parallelly. An Isobaric pressure exchanger ERD is connected in parallel to the RO unit to conserve the energy from the high pressure concentrate high saline stream which otherwise would be lost. The main boost pump feeds the required sea water at low pressure to both the high-pressure pump and the inlet of the ERD.

The flow diagram of the system is shown below in Figure 3.1.

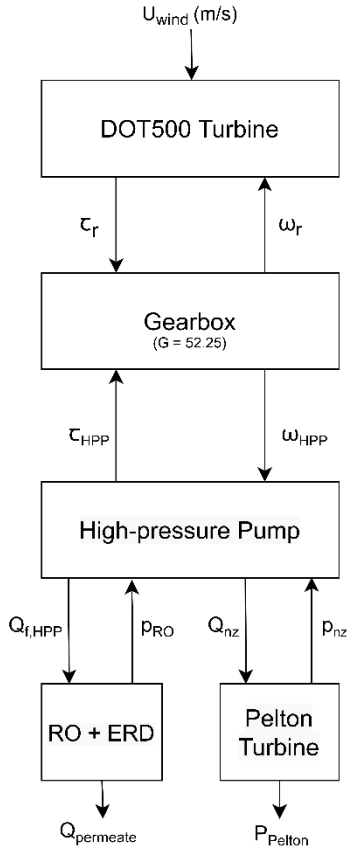

Figure 3. 1 Flow chart of wind powered freshwater production system

The input energy source to the system is the wind at speed U [m/s]. The DOT500 turbine converts this wind energy into rotational speed, ω_r and torque, τ_r of the low speed shaft.

3.1 Model Steady state Equations

The equations used to build a numerical model of the system and simulate at different conditions are explained briefly below.

The ratio between the speed of the tip of the rotor blade and the wind speed, U is called tip speed ratio. It is defined as:

$$\lambda = \frac{\omega_r \cdot R}{U} \tag{3.1}$$

where ω_r is the angular velocity or angular rotational speed of the wind turbine [rad/s] and R is the radius of the turbine rotor swept area and is equal to 22 meters for the DOT500 turbine.

From Equation 3.1, the rotational speed of the low speed shaft, ω_r is given by Equation 3.2:

$$\omega_r = \frac{\lambda \cdot U}{R_{rotor}} \tag{3.2}$$

The torque on the low speed shaft, τ_r is defined by Equation (3.3) below:

$$\tau_r = C_c \cdot \frac{1}{2} \cdot \rho_{air} \cdot \pi \cdot R^3 \cdot U^2 \tag{3.3}$$

where C_c is the coefficient of torque, ρ_{air} is the density of air and is assumed to be a constant of 1.225 [kg/m^3].

The torque-rotational speed characteristics of the DOT500 turbine are plotted from the cut-in wind speed, 3 m/s to the rated wind speed, 12m/s in Figure 3.2 below.

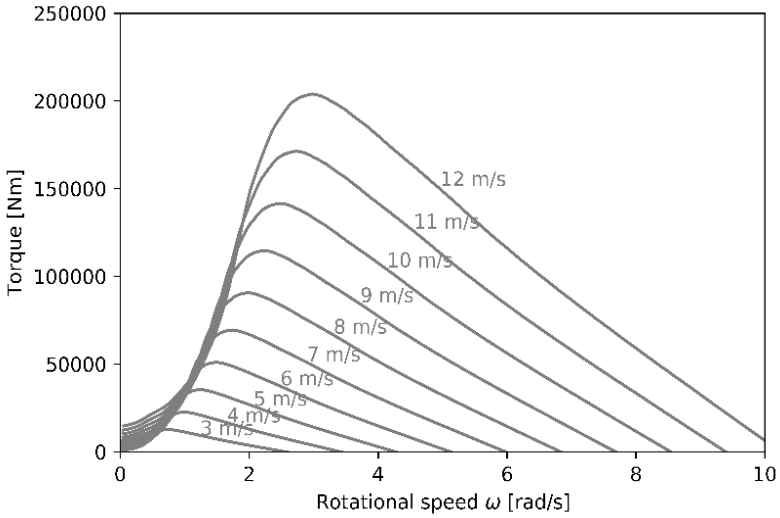

Figure 3. 2 Torque-Rotor speed characteristic of DOT500.

For every wind speed, U, the λ and C_t values from the blue curve in Figure 2.6 are used to obtain the respective rotational speed, $\omega_r(U)$ and torque, $\tau_r(U)$ using Equations 3.2 and 3.3 respectively.

The power harnessed by the wind turbine is thus a product of aerodynamic torque and aerodynamic angular rotational speed of the low speed shaft.

The gearbox increases the rotational speed of the high-speed shaft by a ratio, G. The high-speed shaft rotational speed, ω_{HPP} then becomes:

$$\omega_{HPP} = \omega_r \cdot G \tag{3.4}$$

The torque on the high-speed shaft, τ_{HPP} is reduced by the gearbox ratio G as shown in Equation 3.5 below:

$$\tau_{HPP} = \frac{\tau_r}{G} \cdot \eta_{gearbox} \tag{3.5}$$

where $\eta_{gearbox}$ is the mechanical efficiency of the gearbox.

The high-speed shaft is coupled to the shaft of the high-pressure pump. The torque on the high-speed shaft, τ_{HPP} is translated into pressure of the feed medium (seawater) delivered by the high-pressure pump and is defined by the Equation 3.6 below:

$$\Delta p_{HPP} = \frac{\tau_{HPP} \cdot \eta_{mech,HPP}}{V_{HPP}} \tag{3.6}$$

where V_{HPP} is the volumetric displacement of the pump and is an internal property of the pump in L/rev. $\eta_{mech,HPP}$ is the mechanical efficiency of the high-pressure hydraulic pump.

The high-pressure pump flow rate [m^3/s] is expressed as a function of rotational speed in Equation 3.7:

$$Q_{HPP} = \omega_{HPP} \cdot V_{HPP} \cdot \eta_{vol,HPP} \tag{3.7}$$

where $\eta_{vol,HPP}$ is the volumetric efficiency of the HPP.

The high-pressure pump torque, τ_{HPP} and the rotor speed, ω_r are related as follows:

$$\tau_{HPP} = \frac{Q_{HPP} \cdot \Delta p_{HPP}}{\omega_r} \tag{3.8}$$

The pressure difference over the high-pressure pump is assumed to be equal to the discharge pressure on the output side of the pump i.e. feed flow. This assumption is made because the inlet pressure of feed seawater from the boost pump to high-pressure pump is substantially lower than the discharge pressure. The positive displacement pump is a fixed volume pump and creates a certain flow at certain rotational speed independent of the pressure it operates at.

The division of the flow from the high-pressure hydraulic pump is shown in Figure 3.3 below:

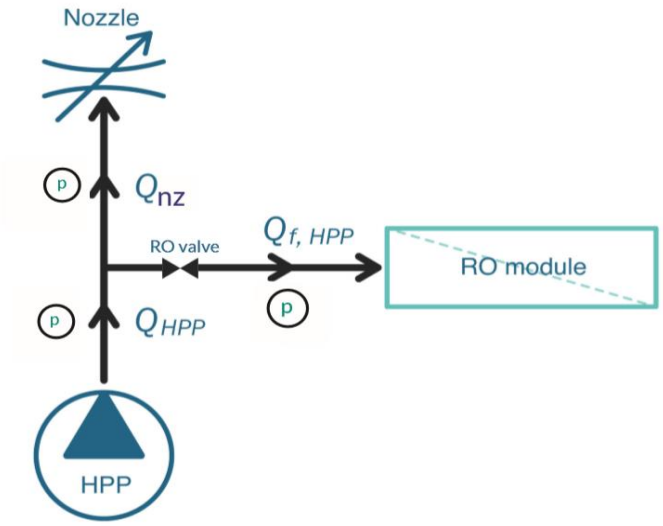

Figure 3. 3 Schematic representation of the flows and pressures from HPP.

The flow from the high-pressure pump, is divided into two streams. $Q_{f,HPP}$ represents the high-pressure pump feed flow to the reverse osmosis membranes and Q_{nz} represents the input stream to the pelton turbine via the nozzle. The pressure of the fluid medium at all the three stream is equal and is controlled by the position of the spear.

$$\Delta p_{HPP} = p_{nz} = p_{RO} = p \tag{3.9}$$

where Δp_{HPP} is defined in Equation 3.6, p_{nz} is the pressure at the spear valve which is a consequence of the position of the nozzle and p_{RO} is the pressure on the feed side of the RO system.

The DOT uses a spear valve as a nozzle to control the pressure. The pressure - flow relation through a spear valve is given by the Equation 3.10 below [19]:

$$Q_{nz} = \sqrt{\frac{2 \cdot \Delta p_{nz}}{\rho_{water}}} \cdot C_d \cdot A_{nz}(s) \tag{3.10}$$

where Δp_{nz} is the pressure drop across the nozzle, ρ_{water} is the density of water, C_d is the coefficient of discharge and is assumed to be 1, $A_{nz}(s)$ is the effective area of the nozzle which depends on the position of the nozzle, s. The term Δp_{nz} can be written as the pressure at the pump side of the nozzle by assuming the pressure at the outlet of the nozzle to be atmospheric.

Figure 2.8 shows the cross section of the spear valve used as a nozzle in the DOT system. The effective area of the nozzle is given by Equation (3.11) below [9]:

$$A_{nz}(s) = \frac{\pi}{4} D_{nz}^2 - [(s \cdot \tan\frac{\alpha}{2})^2 \cdot \pi] \tag{3.11}$$

The range of nozzle position, s varies from 0 mm representing the nozzle to be fully open, the effective nozzle area is maximum, to s equal to 40.745mm representing the nozzle to be fully closed, A_{nz} is 0.

Opening the spear valve results in an increase in the effective nozzle area thus a decrease in pressure. Similarly, closing the spear valve results in the decrease in the effective nozzle area, thus increase in pressure.

Figure 3.4 below shows a schematic representation of the DOT500 system coupled to a RO module with an ERD in parallel and a pelton turbine via the nozzle.

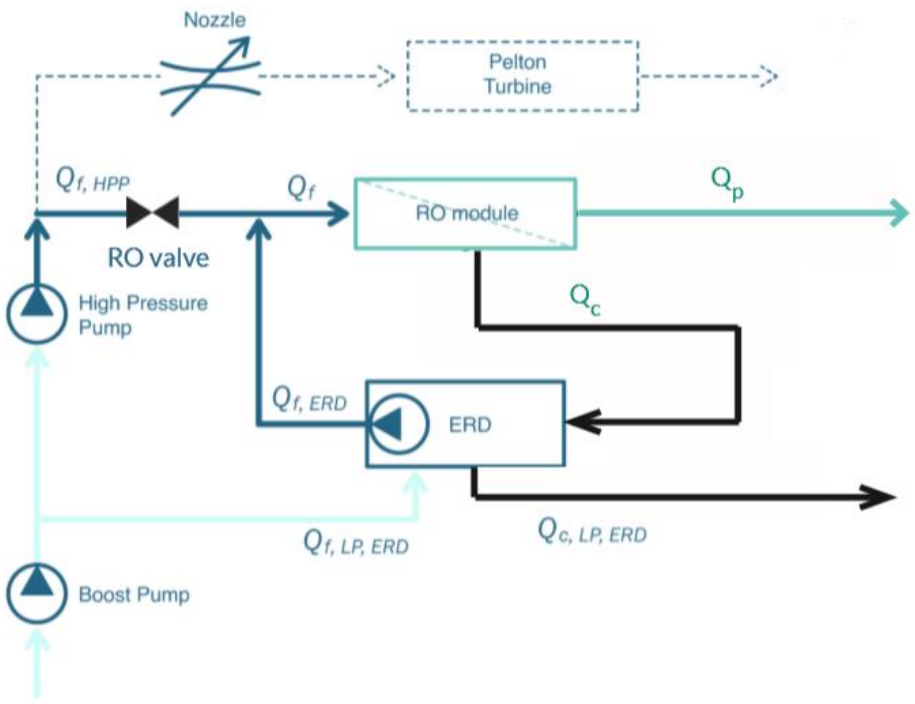

Figure 3. 4 Schematic representation of wind powered RO system with an ERD and Pelton turbine.

The total feed flow of sea water to the reverse osmosis module is made up of two flows as seen in the Figure 3.4 above. $Q_{f, HPP}$ is the pressurized flow coming directly from the high-pressure pump. The second flow, $Q_{f,ERD}$ is the one coming from the ERD.

$$Q_f = Q_{f, HPP} + Q_{f, ERD} \tag{3.12}$$

The operational losses in the ERD system are volumetric mixing (VM) and Leakage (L) [9]. The transfer of energy from the concentrate stream to the feed seawater stream occurs without a physical barrier. This leads to some amount of mixing of concentrate stream into the seawater stream known as volumetric mixing. To account for the volumetric mixing, excess seawater has to be supplied to clear the chambers of the rotary cylinder of the ERD. This is known as overflush (OF). Leakage is a loss which occurs at the seals of the isobaric chambers within the ERD [27].

These operational losses are accounted for in the model by increasing the flow rate of the feed from the boost pump to the ERD, $Q_{f,lp,ERD}$ proportionally. Thus, the flow rate of the outgoing pressurized feed flow from the ERD to the RO is less than the low-pressure feed flow $Q_{f,lp,ERD}$ by a factor of (OF · L).

Several assumptions are made while constructing a numerical model of the reverse osmosis desalination system. Firstly, the seawater fluid medium is assumed to be incompressible. Thus, the density of seawater remains constant throughout the system. The height of the entire system is considered to be negligible, so that the change in potential energy of the liquid at any point in the system is 0. There is no effect on the density of the fluid medium due to changing salinity in the feed. The friction losses due to the resistance of any valve or pipeline in the system is assumed to be negligible.

To calculate the pressure-flow relation on the RO side of the DOT system several parameters are defined below.

The water flux through the RO membrane, J_w [$\frac{kg}{m^2 s}$], can be expressed as a function of permeability coefficient K_w and net driving pressure as given by Robert Bergman [22]:

$$J_w = (\Delta p - \Delta\pi)\cdot K_w = \frac{Q_p \cdot \rho}{A_m} \tag{3.13}$$

where $\Delta\pi$ is the osmotic pressure difference defined in Equation (3.14) below, Δp is the hydrostatic pressure difference over the membrane and Q_p is the flow rate of permeate stream. The term ($\Delta p - \Delta\pi$) is defined as the net driving pressure and is the actual driving pressure available to force the water through the membrane for salt separation. A_m is the membrane area.

$$\Delta\pi = C_{eff} \cdot R \cdot T \tag{3.14}$$

C_{eff} is the effective average concentration at the surface of the membrane in ppm, R is the gas constant equivalent to the Boltzmann constant and is equal to 8.314 [J/mol] and T is the temperature in Kelvin. The osmotic pressure, $\Delta\pi$ can be expressed as a function of the salinity of the solution. Sea water with a salt concentration of around 32000ppm and Temperature of 25° C has an osmotic pressure of approximately 30 bar. The feed water has to be fed into the RO system at an applied pressure greater than the osmotic pressure of the feed: $p_{applied} > p_{osmotic}$ for the water to be pushed in the right direction through the RO membranes to produce filtered water. The osmotic pressure is dependent on temperature[18].

According to Bartman et al. [20], the expression for pressure on the RO side of the system can be obtained by first calculating the permeate flow. This is obtained by using the water flux through the membrane term in Equation 3.13. It is assumed that the pressure of the concentrate flow is equal to the pressure of the feed stream. Therefore Δp is equal to p_{RO}.

$$Q_p = \frac{A_m \cdot K_w}{\rho} \cdot (p_{RO} - \Delta\pi) \tag{3.15}$$

The pressure on the RO side of the membrane can be obtained by substituting Q_p equal to $Q_{f,HPP}$ in Equation 3.15. This is also by assuming the leakage, L is negligible. The outcome of the model of the ERD circuit and a complete derivation of the same can be found in the study performed by Roy Smith [9].

$$p_{RO} = \frac{\rho_{water}}{A_m \cdot K_w} \cdot Q_{f,\,HPP} + \Delta\pi \tag{3.16}$$

Equation 3.16 can be rearranged to define the feed flow from the HPP to the RO unit:

$$Q_{f,\,HPP} = (p_{RO} - \Delta\pi) \cdot \frac{A_m \cdot K_w}{\rho_w} \tag{3.17}$$

It can be observed in Figure 3.3, that the flow from the high-pressure pump, Q_{HPP} is equal to the summation of flow to the pelton turbine, Q_{nz} and high-pressure pump feed flow to the RO system, $Q_{f,HPP}$. This is according to the conservation of mass and is defined in the Equation 3.18 below:

$$Q_{HPP} = Q_{nz} + Q_{f,HPP} \tag{3.18}$$

Substituting Q_{nz} and $Q_{f,HPP}$ from Equations 3.10 and 3.17 in Equation 3.18 leads to:

$$Q_{HPP} = \sqrt{\frac{2 \cdot \Delta p_{nz}}{\rho_{water}}} \cdot C_d \cdot A_{nz}(s) + (p_{RO} - \Delta\pi) \cdot \frac{A_m \cdot K_w}{\rho_w} \quad (3.19)$$

here $\sqrt{\frac{2}{\rho_{water}}} \cdot C_d$ and $\frac{A_m \cdot K_w}{\rho_w}$ are constants and can be replaced by K_1 and K_2 respectively.

Since the pressure of the fluid medium is equal at all 3 nodes as p as described in Equation 3.9, Equation 3.19 becomes:

$$Q_{HPP} = \sqrt{p} \cdot A_{nz}(s) \cdot K_1 + (p - \Delta\pi) \cdot K_2 \quad (3.20)$$

This gives us a relation between the rotational speed on the high-speed shaft of the hydraulic drive train and the pressure in the system as a consequence of nozzle position, s.

For pressures below osmotic pressure, the RO valve is closed. This results in the flow from the high-pressure pump to completely flow towards the pelton turbine generator via the nozzle. Hence the high-pressure pump feed flow to the RO system, $Q_{f,HPP}$ is 0. For the model with the RO valve closed at low operating pressures in the system, Equation 3.20 becomes:

$$Q_{HPP} = \sqrt{p} \cdot A_{nz}(s) \cdot K_1 \quad (3.21)$$

For any given wind speed and any given nozzle position, the pressure in the system can be solved using Equations 3.20 and 3.21. This is discussed in further detail in the algorithm for solving flows below.

3.2 Algorithm for solving flows:

To solve the system of flow rate equations, an algorithm is coded in Python. This solves for the pressure in the system at any given wind speed, U and for any given nozzle position, s. The working principles of the algorithm are illustrated by figure 3.5 below. When going through the steps of the algorithm below, elements of the figure below will be further explained, and it will become clear how the figure visualizes the solution strategy.

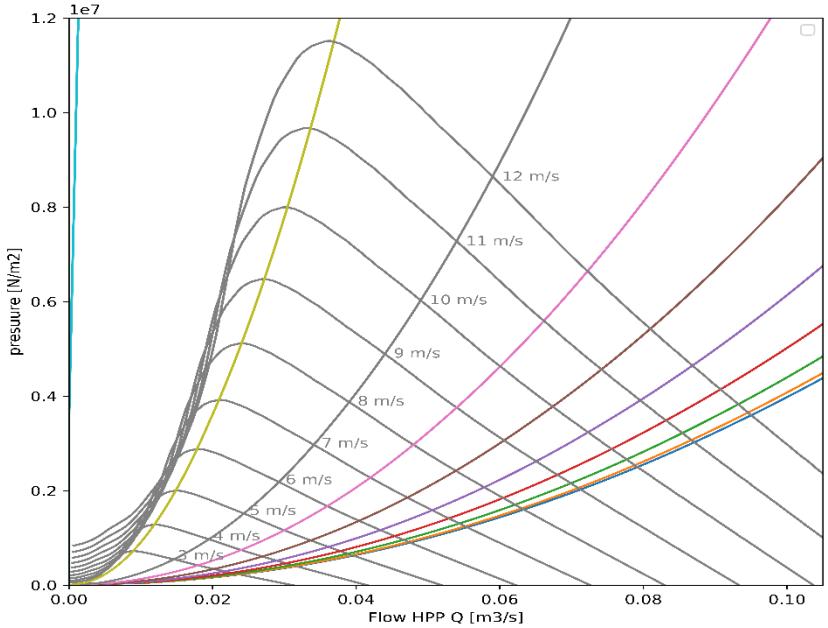

Figure 3. 5 Pressure – Flow relation of DOT500 at different wind speeds and nozzle positions.

1. From the input wind speed, the aerodynamic rotational speed at that particular wind speed is calculated by using Equation 3.2, for the range of tip speed ratios between 0 and 18, where the wind speed can produce power.

2. The aerodynamic torque is calculated at the input wind speed using Equation 3.3 and tabulated values of C_c as shown graphically in figure 2.6. This is again done for tip speed ratios between 0 and 18.

3. The aerodynamic rotational speed is translated into flow of the high-pressure pump using Equation 3.7.

4. The aerodynamic torque is translated into pressure of the high-pressure pump using Equation 3.6. The result of step 3 and step 4 is visualized in Figure 3.5, as the grey line for a particular wind speed. This represents the rotor characteristic in terms of a pressure-flow relation at the high-pressure pump.

5. The high-pressure pump flow and pressure values are split into 2 vectors each, based on the maximum value situated at the peak of the pressure-flow relation of individual wind speeds.

6. For the input nozzle position, s the corresponding effective area of the nozzle, A_{nz} is calculated using Equation 3.11.

7. The pressure values calculated in step 4 are input into Equation 3.21 for pressures below osmotic pressure and Equation 3.20 for pressures above osmotic pressure. The result of this step for nozzle positions at equal intervals of 4.55mm within its operating range is shown by the colored lines in figure 3.5.

8. For a given wind speed and nozzle position, the operation of the system will be at the equilibrium point of intersection of the two lines obtained in step 4 and step 7.

9. Newton Raphson method is used to find the intersection point by finding the root of the non-linear function defined in equation 3.20 for pressures above osmotic pressure and equation 3.21 for pressures below osmotic pressure. This method solves iteratively using both the function and the derivative of the function by making an initial guess of the root.

10. The search for an intersection between the curves obtained in step 4 and 7 is divided to the left and to the right of the peak of the rotor characteristics graph in Figure 3.5. This is because the Newton-Raphson method uses the derivative of the function to find the root.

11. If the operation of the system falls at an equilibrium point between the data points determined by the tabulated values of C_τ - λ, linear interpolation is used.

12. The corresponding value of Q_{nz} for pressures below osmotic pressure and Q_{nz} and $Q_{f,HPP}$ for pressures above osmotic pressure are calculated using equations 3.10 and 3.17 using the pressure solution at the high-pressure pump.

Electricity is generated by impinging the high-pressure flow through the nozzle into a pelton turbine wheel. A generator is coupled to the turbine wheel shaft to generate electricity. The turbine extracts energy from the impulse of high-pressure water. The jet water from the nozzle strikes the vanes (buckets) of the pelton wheel. This causes the runner to rotate at high speeds. The rotational speed of the pelton wheel, ω_{Pelton} [rad/s] as a function of the flow rate through the nozzle, Q_{nz} is given in the Equation 3.22 below:

$$\omega_{Pelton} = \frac{Q_{nz} \cdot \eta_{vol,Pelton}}{V_{pelton}} \tag{3.22}$$

where $\eta_{vol,Pelton}$ is the volumetric efficiency of the pelton turbine and is assumed to be 97% and V_{Pelton} is the volumetric displacement of the pelton motor in [m^3/rev]. The pelton motor used in the DOT system has a volumetric displacement of $2.25 \cdot 10^{-4}$ [m^3/ rev.] or $3.58 \cdot 10^{-5}$ [m^3/ rad].

The torque (N-m) generated in the pelton wheel shaft is given by Equation 3.23:

$$\tau_{Pelton} = V_{Pelton} \cdot p_{nz} \cdot \eta_{mech,Pelton} \tag{3.23}$$

where p_{nz} is the pressure generated due to the flow through the nozzle and is a function of nozzle position and $\eta_{mech,Pelton}$ is the mechanical efficiency of the pelton turbine and is assumed to be 97% for all operating ranges.

The generator coupled to the shaft of the turbine runner wheel converts the mechanical (rotational) energy of the shaft into electrical energy. The power generated by the generator in kW is given by:

$$P_{Pelton} = \tau_{Pelton} \cdot \omega_{Pelton} \tag{3.24}$$

The reverse osmosis system consists of multiple pressure vessels in a parallel configuration and multiple membranes inside each vessel in a series configuration. For the steady state, the RO system is modeled as one single unit.

The total feed to the RO system, Q_f is the summation of the flow coming directly from the high-pressure pump , $Q_{f,HPP}$ and the pressurized flow coming from the ERD, $Q_{f,\ ERD}$ as defined in Equation 3.12. The feed flow to the RO coming from the ERD, $Q_{f,ERD}$ is equal to the concentrate flow rate from just the high-pressure pump feed, $Q_{f,\ HPP}$. Thus, Equation 3.12 becomes:

$$Q_f = Q_{f,HPP} + (1 - \gamma) \cdot Q_{f,HPP} \quad (3.25)$$

where γ is the recovery rate of the RO system. The term $(1 - \gamma) \cdot Q_{f,HPP}$ is the input of pressurized concentrate feed to the ERD.

The total permeate flow rate, Q_p is the recovery rate, γ times total feed flow to the RO system, Q_f and is defined in Equation 3.26 below:

$$Q_p = \gamma \cdot Q_f \quad (3.26)$$

The maximum permeate that can be produced by entire RO system, $Q_{p,\,max}$ is defined below:

$$Q_{p,\,max} = Q_{p,\,mem,\,max} \cdot n_{mem} \cdot n_{vessel} \quad (3.27)$$

where n_{mem} is the number of membranes per pressure vessel, n_{vessel} is the number of vessels in the RO system and $Q_{p,\,mem,\,max}$ is the maximum permeate that can be produced by a single membrane. The main reason for using multiple membranes inside each vessel is to increase the recovery rate of permeate from the feed seawater. The maximum operating pressure of the entire RO system is limited by the maximum allowable applied pressure of a single membrane.

The flow rate of the boost pump, Q_{boost} is defined Equation 3.28 below:

$$Q_{boost} = Q_{HPP} + Q_{f,\,LP,\,ERD} \quad (3.28)$$

where Q_{HPP} is the flow rate of the high-pressure pump and $Q_{f,\,LP,\,ERD}$ is the low-pressure feed flow from the boost pump to the ERD and can be written in terms of high-pressure pump feed to the RO, $Q_{f,\,HPP}$ and recovery rate as in Equation 3.29 for simplification. The losses within the ERD are taken into account.

$$Q_{boost} = Q_{HPP} + \frac{(Q_{f,HPP} \cdot (1 - \gamma))}{\eta_{ERD}} \quad (3.29)$$

where η_{ERD} can be defined as the total efficiency of the ERD system and is given by the Equation below:

$$\eta_{ERD} = (1 - OF) \cdot (1 - L) \quad (3.30)$$

OF is the overflush and L is the leakage within the ERD.

3.3 Power consumption model

The main objective of this model is to calculate the power consumed by the system per cubic meter of seawater pumped into the system and per cubic meter of permeate produced.

Power consumed in kW per cubic meter of seawater pumped into the system at a given wind speed U, is given by Equation 3.31:

$$P_{m3}(U) = \frac{P_{total}(U)}{Q_{total}(U)} \quad (3.31)$$

where $P_{total}(U)$ is the total power consumed at wind speed, U by the entire system including the ERD, the boost pump and the sensors used. The power consumed by the ERD is the power of the boost pump

feeding seawater to the ERD and the power required to rotate the ERD rotor. The power required to rotate the rotor is independent of the pressure difference between low-pressure feed seawater and high-pressure concentrate stream. The exact relation between the rotational speed and power consumed is not known from the datasheet and hence it is assumed to be constant at its rated power. Hence, P_{total} is given by the Equation 3.32 below:

$$P_{total}(U) = P_{ERD}(U) + P_{boost}(U) + P_{sensor} \tag{3.32}$$

The power consumed in kW by the boost pump per cubic meter of seawater pumped at wind speed, U is defined by Equation 3.33 below:

$$P_{boost}(U) = \frac{Q_{HPP}(U) \cdot \Delta p_{boost}(U)}{\eta_{mech,boost} \cdot \eta_{vol,boost}} \tag{3.33}$$

where Q_{HPP} (U) is the flow rate from the boost to the high-pressure pump at wind speed U, $\eta_{mech,boost}$ is the mechanical efficiency and $\eta_{vol,boost}$ is the volumetric efficiency of the boost pump. $\Delta p_{boost}(U)$ is the pressure difference between the inlet and the outlet feed in the boost pump at wind speed U and is defined in Equation 3.34 below:

$$\Delta p_{boost}(U) = p_{f,boost}(U) - p_{atm} \tag{3.34}$$

where $p_{f,boost}$ is the pressure of the seawater pumped by the boost pump from the ocean to high-pressure pump and low-pressure feed inlet of the ERD. $p_{f,boost}$ is assumed to be a constant 7 bar at all wind speeds. p_{atm} is the atmospheric pressure on the inlet side of the boost pump and is assumed to be 1 bar.

Chapter 4: Simulation of Wind powered Reverse Osmosis system

Using the equations and algorithm defined in Chapter 3, simulations are performed for different scenarios and the results are analyzed in this chapter.

4.1 Simulation of the model for maximum turbine power

First a simulation is performed for the model shown in Figure 1.1 for the control of the DOT500 turbine for maximum turbine power between cut-in wind speed, $U_{cut\text{-}in}$ and rated wind speed, U_{rated}. This maximum power point tracking control curve, K_{opt} shown in figure 4.1 below (blue curve) allows the wind turbine to extract as much power as possible for every wind speed below U_{rated}.

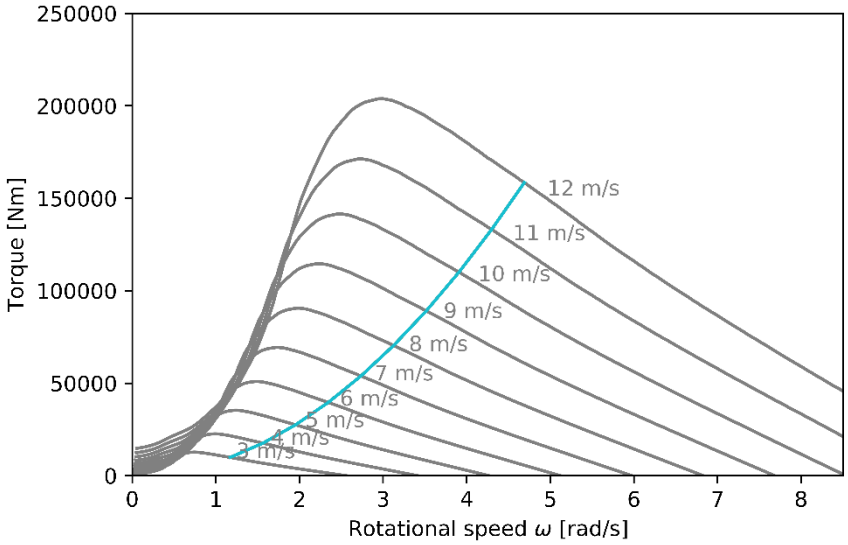

Figure 4. 1 Torque- Rotational speed behavior of the DOT500 turbine with K_{opt} curve (blue).

K_{opt} is defined in the Equation 4.1 below:

$$K_{opt} = \frac{1}{2}\cdot\rho\cdot\pi R^5\cdot\left(\frac{C_{p,max}}{\lambda_{opt}^5}\right) \quad (4.1)$$

where $C_{p,max}$ is the maximum power coefficient and it is a characteristic of the wind turbine and λ_{opt} is the tip speed ratio at the maximum power coefficient.

The power coefficient, C_p and the torque coefficient, C_τ curves at different tip speed ratios for the DOT500 hydraulic drive train wind turbine are plotted in Figure 2.6. To realize the analysis of a wind turbine for required operation at a specific tip speed ratio, the rotor performance in terms of C_p and C_τ over all expected tip speed ratios needs to be plotted. These curves determine the performance of the rotor. The maximum power is extracted at λ_{opt} equal to 8.6 and the corresponding $C_{p,max}$ value is 0.462.

At every wind speed, the optimum rotational speed, ω_{opt} for maximum power extraction becomes:

$$\omega_{opt} = \frac{\lambda_{opt}\cdot U}{R_{rotor}} \quad (4.2)$$

The torque is directly proportional to the square of the rotational speed and is defined by the parabolic equation below:

$$\tau_{opt} = K_{opt} \cdot \omega_{opt}^2 \quad (4.3)$$

At every wind speed, the torque and rotational speed points lie on the blue curve in Figure 4.1. Hence it is assumed that the high-pressure pump delivers the corresponding flow and pressure at every wind speed. At any point in the operation of this system, if the RO membrane limits are exceeded, the RO valve is closed to prevent damage to the RO unit. The behavior of the DOT desalination system with a pelton turbine is simulated and the results are shown below.

For the simulation several system parameters are kept constant and are shown in Table 4.1 below:

Table 4. 1: System parameters and constants used for modeling.

System Parameter	Value / Type
Membrane used	LG SW 440 R
Active area of the membrane, A_{mem}	41 m^2
Maximum allowable membrane pressure, $p_{mem\ max}$	82.7 bar
Maximum permeate production per membrane, $Q_{p,max}$	37 m^3 / day
Number of membranes per pressure vessel, n_{mem}	6
Number of pressure vessels, n_{vessel}	6
Recovery rate, γ	42%
Permeability coefficient, K_w	$4.166 \cdot 10^{-9}$ s/m
Concentration of feed seawater, C_{feed}	32000 mg/L
Volumetric displacement of HPP, V_{HPP}	1.61 L /rev.
Nominal pressure of HPP, $p_{nom,HPP}$	160 bar
Spear valve nozzle diameter, D_{nz}	38mm
Coefficient of discharge of nozzle, C_d	1
Volumetric displacement of Pelton, V_{Pelton}	$2.25 \cdot 10^{-4}$ m^3/ rev.
Nominal pressure of Pelton turbine, $p_{nom,Pelton}$	160 bar
ERD used	Danfoss iSave 40
Volumetric displacement of ERD, V_{ERD}	$626 \cdot 10^{-6}$ m^3/rev.
Maximum rotational speed of ERD, $\omega_{max,\ ERD}$	1200 rpm
Flow rate range of ERD, $Q_{f,\ LP,\ ERD}$	21 – 41 m^3/h
Leakage coefficient, L	0.01
Overflush coefficient, OF	0.01
Density of air, ρ_{air}	1.225 kg/m^3
Density of water, ρ_{water}	1025 kg/ m^3
Temperature of feed water, T	25° C
Volumetric efficiency of HPP, $\eta_{v,\ HPP}$	95 %
Mechanical efficiency of HPP, $\eta_{m,\ HPP}$	80%
Volumetric efficiency of Pelton, $\eta_{v,\ Pelton}$	97%
Mechanical efficiency of Pelton, $\eta_{m,\ Pelton}$	95%
Gearbox efficiency, $\eta_{gearbox}$	95%
Generator efficiency, $\eta_{generator}$	95%

For the steady state model calculations, the membrane permeability coefficient, K_w is assumed to be a constant. In reality, since the system operates at varying pressures, concentrations and temperatures, the value of K_w varies over time. Its value mainly depends on the thickness of the membrane, its pore size, shape and porosity. Generally, K_w is obtained experimentally, since it is influenced by the type of membrane used.

The position of the spear valve used as a mechanism to control the pressure is shown in Figure 4.2 below. The red curve indicates the spear position at different wind speeds below rated wind speed and the blue curve indicates the pressure in the system as a result of the resistance created by the nozzle at that particular spear position s.

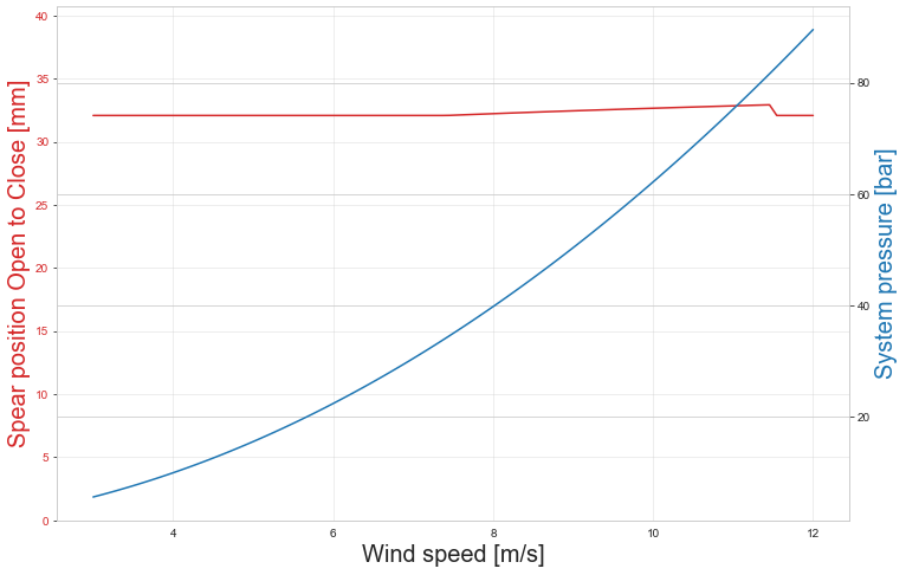

Figure 4. 2 Spear position at different wind speeds and corresponding pressure.

As seen in the blue curve, at pressures below osmotic pressure (34 bar), the position of the nozzle indicated by the red curve remains constant. The flow rate of water through the RO valve is directly proportional to the pressure above osmotic pressure. Once the osmotic pressure is reached, the nozzle moves slightly towards the close position. This is due to the opening of the RO valve for water production. The nozzle needs to move slightly towards close position to reduce the effective area, to keep the pressure at the desired level. At 11.6 m/s, the pressure limit of the RO membranes is reached, and the control strategy is to close the RO valve. This is done to maintain operation on the K_{opt} curve. This results in the position of the spear valve to jump back to its original position of operation for wind speeds below which osmotic pressure is reached.

The flow rates of the high-pressure pump, feed stream to the RO membranes and flow through a nozzle are plotted for each wind speed in Figure 4.3.

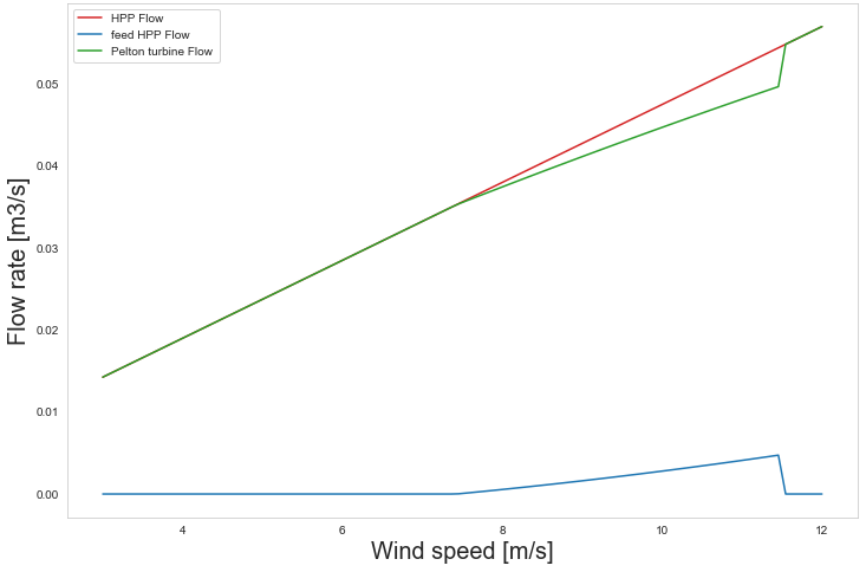

Figure 4. 3 Flow rates at different wind speeds.

The red line indicates the flow through the high-pressure pump. The pump flow rate exhibits linear behavior because positive displacement pumps are constant volume pumps. These pumps provide a constant flow at fixed speeds. A positive displacement pump makes a fluid move by trapping a fixed volume of fluid and displacing the trapped volume into the discharge pipe. Therefore, as the wind speed increases, the rotational speed of the rotor and consequently the high-speed shaft increases linearly according to Equation 4.2, and hence the volume displaced from the pump increases linearly.

The blue curve indicates the high-pressure pump feed flow, $Q_{f,HPP}$ to the RO membrane system. Up to a wind speed of 7.5 m/s there is no flow to the RO because the pressure produced by the high-pressure pump is lower than the osmotic pressure and hence the separation of salts from the feed seawater is not possible. If the feed water is forced through the RO membranes at pressures lower than the osmotic pressure, osmosis will occur and thus the permeate will be consumed. Above osmotic pressure, i.e. above 7.5 m/s the flow to the RO varies according to Equation 3.17. At pressures above the membrane limit at 11.6 m/s, the flow from the high-pressure pump to the RO is cut off to prevent damage to the membranes, as seen in the figure above. All the flow from the high-pressure pump is directed towards the pelton turbine represented by the green curve.

The boost pump pumps the feed seawater at low pressure to both the high-pressure pump and the ERD low pressure feed inlet. The behavior of the boost pump is shown in Figure 4.4 below.

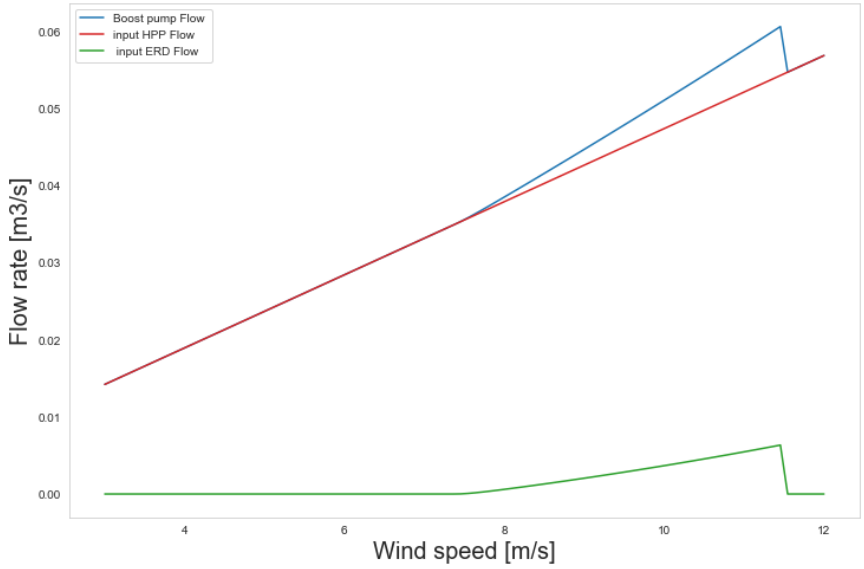

Figure 4. 4 Behavior of the boost pump.

The blue curve represents the flow rate of the boost pump. At pressures lower than the osmotic pressure, all the flow pumped by the boost pump is directed towards the high-pressure pump represented by the red curve. Hence, both the blue and green curves overlap. The RO system does not operate at these lower pressures and as a consequence the ERD also remains non-operational. Hence, the input flow to the ERD is 0 as seen in the green curve. The linear behavior of the high-pressure pump as seen in Figure 4.3 is exhibited by the red high-pressure pump curve. At pressures above the osmotic pressure, the feed is permitted to the ERD and thus the increase in flow rates is seen at both the ERD flow curve and the boost flow curve. When the pressure and/or flow limits of the RO membrane are exceeded, the control strategy causes the closing of the RO valve . This behavior is visible at 11.6 m/s where the ERD flow to the RO input drops to 0.

At every wind speed, water production and electricity generation is plotted in Figure 4.5 if the hydraulic drive train wind turbine follows the K_{opt} control curve.

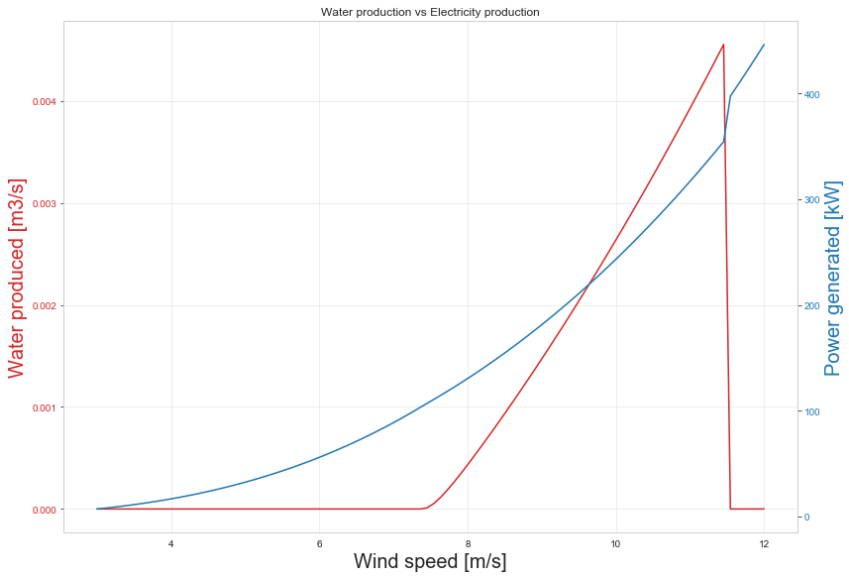

Figure 4. 5 Water production [m3/s] and electricity generation [kW] vs Wind speed [m/s].

The red curve indicates the flow rate of permeate produced as an output of reverse osmosis operation.

The electricity generated by the turbine is represented by the blue curve. At 7.5 m/s when the valve for RO is opened, there is a slight drop in the production of power, due to the diversion of water from high-pressure pump side to the RO side. This causes the slope of the curve at this point to decrease. An increase in the power generation is seen at 11.6 m/s indicating the closing of RO valve due to exceedance of RO system limits.

For the calculation of system power consumption, the assumptions made are shown in Table 4.2 below:

Table 4. 2: Assumptions made for calculation of system power consumption.

System Parameter	Value / number
Power consumed by each sensor, P_{sensor}	5.5 W
Number of pressure sensors, n_p	5
Number of flow sensors, n_Q	4
Number of temperature sensors, n_T	2
Number of concentration sensors, n_c	2

A plot of power generated by the pelton turbine, power consumed by the entire system and power delivered to the grid is plotted for every wind speed in Figure 4.6:

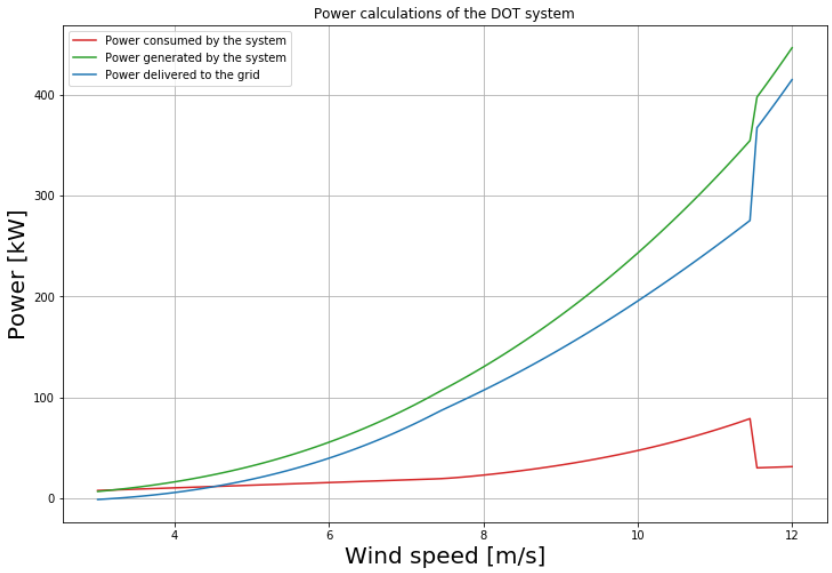

Figure 4. 6 Power generation and consumption at different wind speeds for K_{opt}.

For the turbine operating on the K_{opt} curve, for a wide range of wind speeds, the power generated by the system shown in green is greater than power consumed by the system. At higher wind speeds, the system generates much more power than it consumes. This excess power shown in blue, can either be delivered to the grid or stored in batteries to make the system fully autonomous. This is possible if the total system consumption is managed in a way that the power generated at any given time plus the power stored in the batteries is always greater than the total power consumed by the entire system at any given time. No external supply from the grid is required even at wind speeds near cut-in wind speed because the power generated is equal to the power consumed by the entire system. It can be concluded that if the turbine operates on the K_{opt} curve, it is possible to operate this wind powered reverse osmosis system in an islanded mode.

4.2 Simulation of the model for different operating conditions

For the solved model using the Algorithm, various parameters of the DOT system are plotted against all the nozzle positions from 'Fully-open' position where the position of the nozzle, s is 0 mm to 'Fully-close' position where the position of the nozzle, s is 40.745 mm for wind speeds between $U_{cut\text{-}in}$ and U_{rated}.

The pressure in the system at all nozzle positions is shown in Figure 4.7 below:

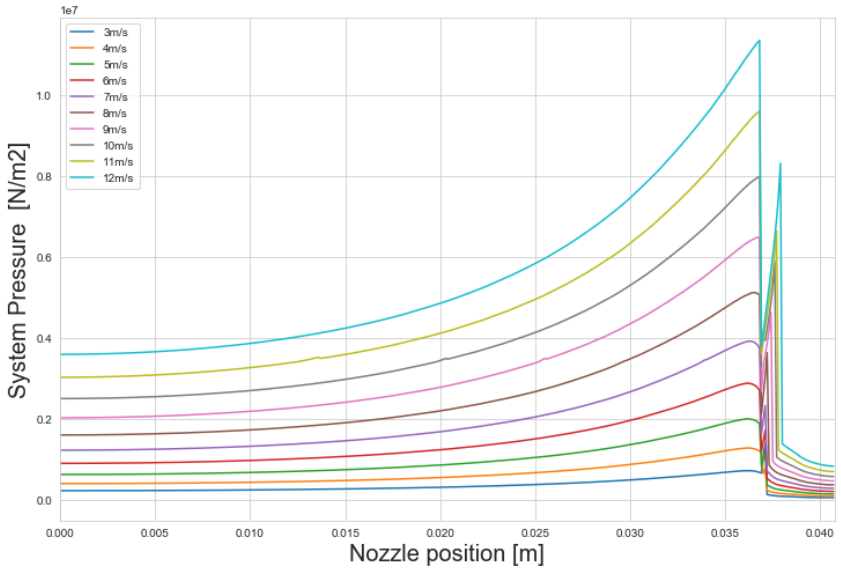

Figure 4. 7 System pressure at all nozzle positions for different wind speed conditions.

The bottom curve represents the cut-in wind speed, 3 m/s and the top blue curve represents the rated wind speed, 12 m/s. From the Figure above, it can be observed that as the nozzle moves from the position of fully open, s equal to 0 mm towards closing position, the pressure in the system is increasing. The system pressure is low for s equal to 0 mm, because at a given wind speed for an open nozzle position, the nozzle curve, shown in Figure 3.5, intersects at a lower torque in the torque-rotational speed/pressure-flow curve for that given wind speed. As the position of the nozzle is moved towards closing position, the intersection of the nozzle curve occurs at a higher torque resulting in a higher pressure in the system.

A sudden drop in the pressure is seen for every wind speed after a certain nozzle position. This is because for nozzle positions above 36.5 mm, the nozzle curve intersects with the pressure-flow curve at a lower torque or the system operates at very low tip speed ratios. This region can be considered as an 'unstable' operating region and needs to be avoided during system operation to avoid a sudden drop in pressure and consequently the closure of the RO valve. This also leads to a drop in the torque generated by the pelton turbine and ultimately a loss of power generated. It can be concluded that the production of water for all wind speeds occurs above a horizontal line which represents the osmotic pressure at 34.28 bar (not seen in the Figure). As the wind speed increases, to produce the same volume of water, the system can be operated at further open nozzle positions, hence avoiding the unstable region. Therefore, the operation of the system at low rotational speeds can be avoided. For higher wind speeds, up to a nozzle position of 36.5 mm, the production of water can start much more on the left stable region.

Even though it is recommended to operate the SWRO unit at constant high pressures (60 - 70 bar), the pressure in the system should not be too high to avoid damaging the membranes. Therefore, the DOT system should be operated by keeping the spear valve open at all wind speeds to maintain operation further away from the unstable region.

The flow rate of seawater from the high-pressure pump, Q_{HPP} at all nozzle positions for different wind speeds is shown in Figure 4.8 below:

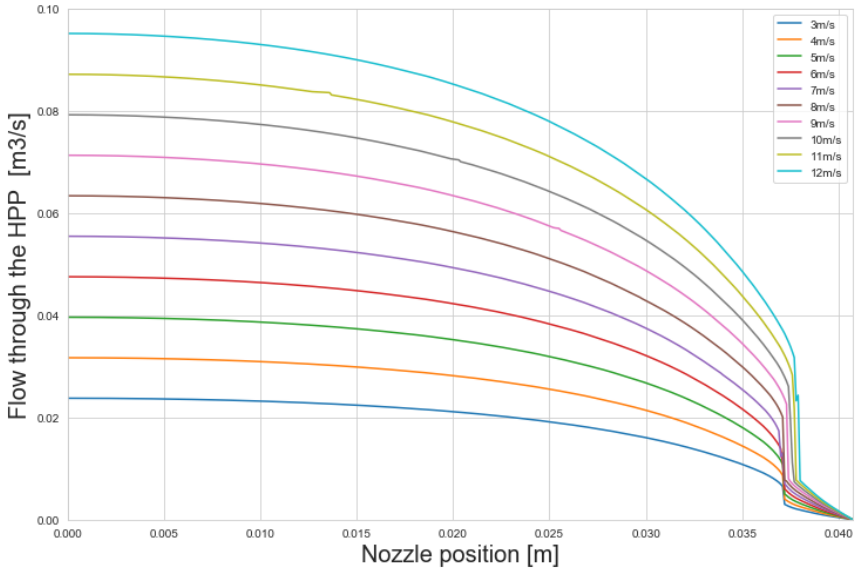

Figure 4. 8 HPP flow at all nozzle positions for different wind speed conditions.

The flow rate of feed seawater from the high-pressure pump is directly proportional to the rotational speed of the high-speed shaft of the hydraulic drive train of the DOT500 wind turbine according to Equation 3.7.The higher the rotational speed, the higher the flow rate of water from the high-pressure pump towards either the spear valve or the RO unit depending on the desired mode of operation. Figure 3.5 shows that at a fully-open nozzle position, i.e. at s equal to 0 mm, the intersection of the nozzle curve occurs at the maximum rotational speed. This translates to maximum high-pressure pump flow at a fixed wind speed for fully-open nozzle position. As the position of the nozzle moves from fully-open towards close, up to the nozzle position, s equal to 37.5 mm, the intersection of nozzle curve with the pressure-flow curve at a particular wind speed occurs at decreasing rotational speed. This explains the decreasing flow caused due to the closing of the spear valve.

For nozzle positions, 37.5 mm $< s <$ 40.745 mm (Fully-close), the nozzle curves tend to have a higher slope and intersect at low rotational speeds on the bottom left corner of Figure 3.5. The wind turbine at this region is operating at low tip speed ratios and hence the high-pressure pump flow drops. This region is the 'unstable' region that was discussed before.

The feed flow to the RO from the high-pressure pump, $Q_{f,HPP}$ at all nozzle positions for different wind speeds is shown in Figure 4.9 below:

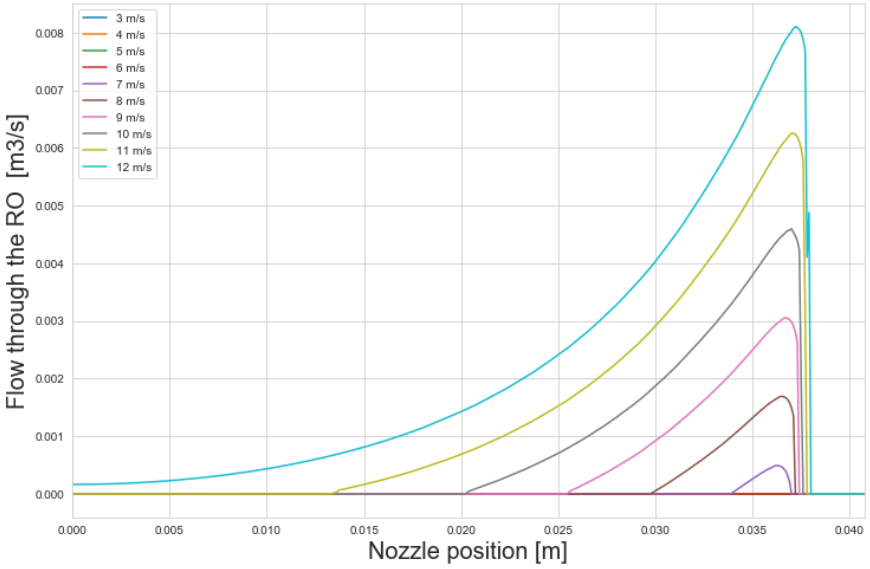

Figure 4. 9 RO flows at all nozzle positions for different wind speed conditions.

Osmotic pressure is reached at a wind speed of 6.54 m/s. For the DOT500 turbine, this is the minimum wind speed at which the system can operate at pressures above osmotic pressure. For wind speeds below this, production of water is not possible. For wind speeds above 6.54 m/s, water can be produced at certain nozzle positions which intersect with the pressure-flow curves at a higher torque value translating to above osmotic pressure. As the wind speed increases, water can be produced at a larger range of nozzle positions. This is because as the wind speed increases, a larger range of nozzle flow curves intersect with the pressure-flow curves above the osmotic pressure. At wind speeds close to the rated wind speed, production of water is possible even at fully open nozzle position. Production of water is not possible between the nozzle range of 38 mm to fully close position due to the operation of the turbine at very low tip speed ratios. This results in operation of the wind turbine at low rotational speeds and consequently, lower torque translating to pressures below osmotic pressure.

The flow through the nozzle to the pelton turbine generator, Q_{nz} at all nozzle positions for different wind speeds is shown in Figure 4.10 below:

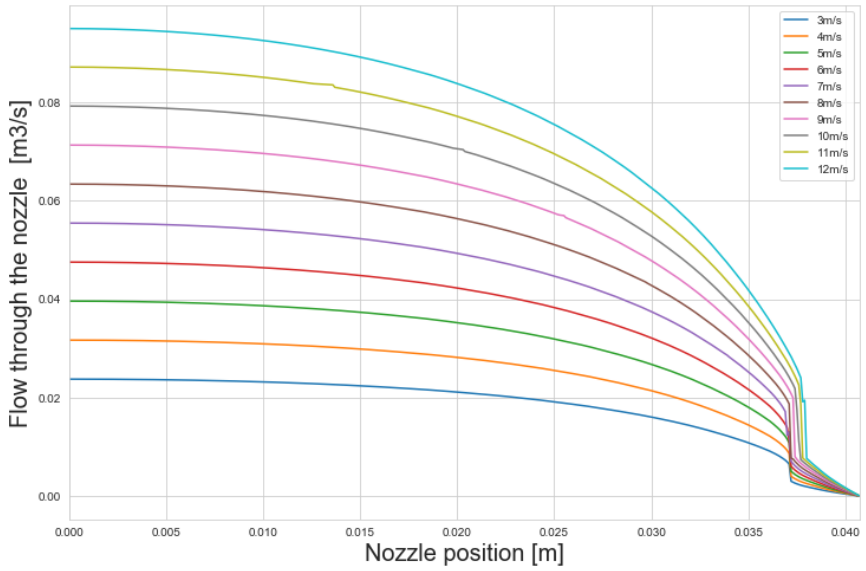

Figure 4. 10 Pelton flows at all nozzle positions for different wind speed conditions.

At nozzle positions between 37.5 mm and fully-close position, the intersection of the nozzle flow curve with the pressure-flow curve of the high-pressure pump occurs at lower rotational speeds of the DOT500 turbine. This results in the drastic reduction of the high-pressure pump flow rate which is directly proportional to the rotational speed of the high-speed shaft, since it is a fixed-volume positive displacement pump. Consequently, this results in a drop of the flow through the nozzle as seen in Figure 4.10.

The flow rate of seawater through the spear valve, Q_{nz} is converted into rotational speed of the pelton turbine. The rotational speed of the pelton wheel, ω_{Pelton} at all nozzle positions for different wind speeds is shown in Figure 4.11 below:

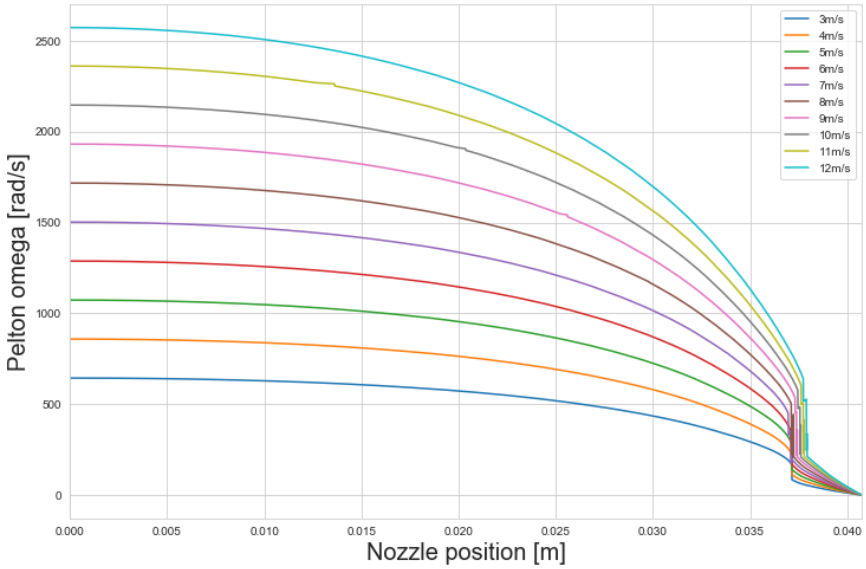

Figure 4. 11 Pelton rotational speed at all nozzle positions for different wind speed conditions.

The nozzle effective area decreases as the nozzle moves towards close position and consequently the flow through the nozzle leading to a decrease in the rotational speed generated in the pelton turbine.

The pressure in the system as a consequence of the nozzle position is translated into torque of the pelton turbine. The torque of the pelton turbine, τ_{Pelton} at all nozzle positions for different wind speeds is shown in Figure 4.12 below:

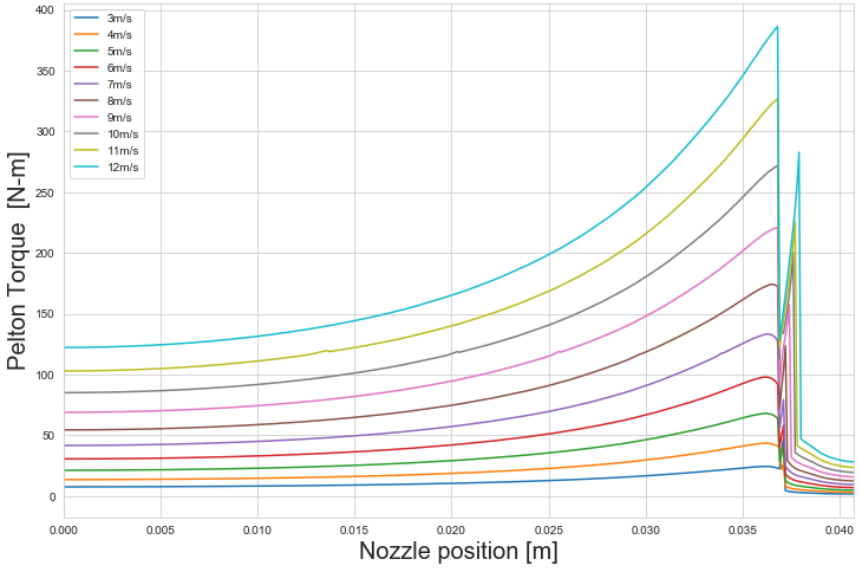

Figure 4. 12 Pelton torque at all nozzle positions for different wind speed conditions.

For nozzle positions between 36.5 mm and fully close position of 40.745 mm, the unstable operating region is visible in Figure 4.12 due to the operation of the DOT500 turbine at low rotational speeds. Operating in this region leads to a loss of power generated in the pelton turbine wheel and hence should be avoided.

Finally, the power generated by the pelton wheel, P_{Pelton} [kW] at all nozzle positions for different wind speeds is shown in Figure 4.13 below:

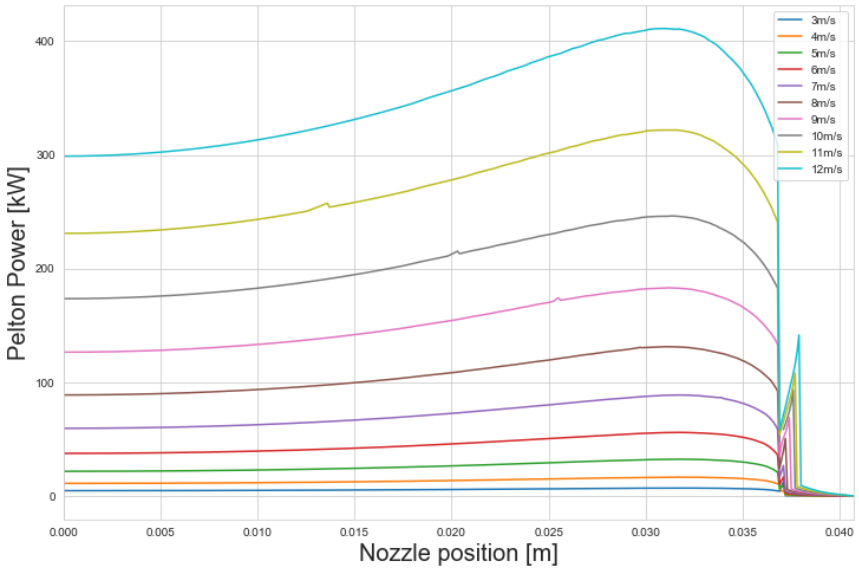

Figure 4. 13 Power generated by pelton turbine at all nozzle positions for different wind speeds.

A kink in the power generated curves can be observed for the operation of the spear valve at nozzle positions in the unstable region due to the intersection of the nozzle curves with the pressure-flow curves at higher pressures. Therefore, the torque generated also varies. An efficiency of 95% is assumed for all ranges of operation accounting for frictional, separation and leakage losses during conversion of energy in the turbine. It can be observed that when the system operates at a particular constant nozzle position, the power generated by the pelton turbine is maximum for all wind speeds. The DOT500 turbine operates on the K_{opt} curve at this position of the nozzle for maximum power extraction from the wind.

Chapter 5: Optimization of the system

The system in Figure 1.1 is optimized for maximum electricity production and maximum water production using an algorithm written in Python. Various system parameters like the pressure, position of the nozzle for different wind speeds, torque and rotational speed of the pelton turbine, revenues from water and electricity production and the control curve on the DOT500 turbine are plotted and analyzed.

For optimization of both maximum water production and electricity production the system parameters mentioned in Table 4.1 are kept constant. Additionally, the parameters kept constant for optimization are described in Table 5.1 below:

Table 5. 1: System parameters and limits considered for optimization.

System Parameter	Value / Type
HPP model and type	Kamat Quintuplex Plunger Pump K 80000 – 5G
HPP flow limit, $Q_{HPP\ max}$	2417 L/min
HPP rated rotational speed, $\omega_{HPP\ rated}$	1500 rpm

5.1 Optimization for Maximum Electricity Production

The wind powered freshwater production system is first optimized for maximum electricity production by closing the RO valve at all wind speeds. An algorithm is written in Python language which first solves the system using the existing algorithm described in chapter 3 for solving flows.

The algorithm gives the pressure and the flow from the high-pressure pump towards the nozzle at all wind speeds and all nozzle positions. The pelton rotational speed, torque and consequently the power generated by the pelton turbine are calculated using Equations 3.22, 3.23 and 3.24 respectively for all wind speeds and all nozzle positions from the pressure and nozzle flow values solved by the algorithm. Since the RO limits do not hold for this type of optimization, the only limit to be considered is the high-pressure pump flow/rotational speed limit. The algorithm searches for the maximum possible power that can be generated at every wind speed for all the nozzle positions between fully-open and fully-close taking into account the high-pressure pump flow/rpm limit.

The control curve for the operation of the DOT500 rotor is plotted in Figure 5.1 below:

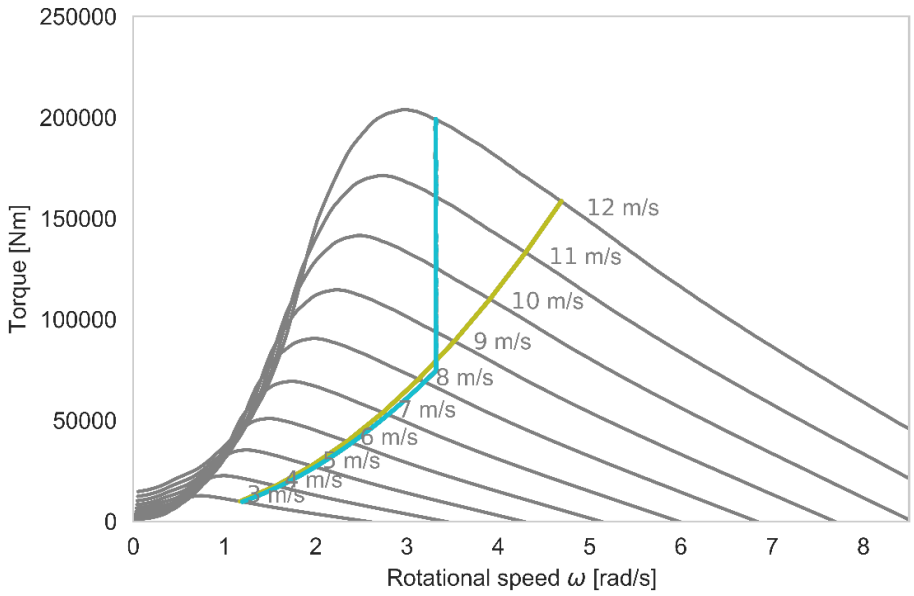

Figure 5. 1 Control curve for DOT500 turbine operation for maximum electricity production.

The aerodynamic torque-rotational speed characteristic of the DOT500 is shown in the grey curves for wind speeds between $U_{cut\text{-}in}$ to U_{rated}. The yellow curve indicates the operation of the turbine for optimum conditions, K_{opt} which indicates the maximum extraction of power from the wind for the given wind speeds. The blue curve shows the control curve if the turbine has to operate to maximize electricity production taking into account all the system limits and efficiencies. Up to the wind speed of 8.29 m/s, at which the flow rate limit of the high-pressure pump is reached, the DOT turbine operates on the K_{opt} curve according to equation 4.3. During this operation, the turbine operates at the maximum coefficient of power equal to 0.462 and the corresponding tip speed ratio of 8.6. A very small deviation is seen from the K_{opt} curve to account for the various losses in the system. The losses include the efficiency of the gearbox, volumetric, mechanical efficiencies of the Kamat high-pressure pump and the pelton turbine. The generator efficiency of the pelton turbine for the conversion of mechanical energy of the turbine wheel to electrical energy is also taken into account. After 8.29 m/s, the rotational speed of the rotor is kept constant to maintain the high-pressure pump flow at the maximum limit. The torque of the rotor is increased up to rated wind speed to increase the pressure in the system, thereby increasing the torque generated in the pelton turbine. This results in the production of maximum electricity within system limits.

The maximum power generated by the pelton turbine generator at every wind speed and subsequently the nozzle position are plotted for wind speeds between $U_{cut\text{-}in}$ and U_{rated} in Figure 5.2 below:

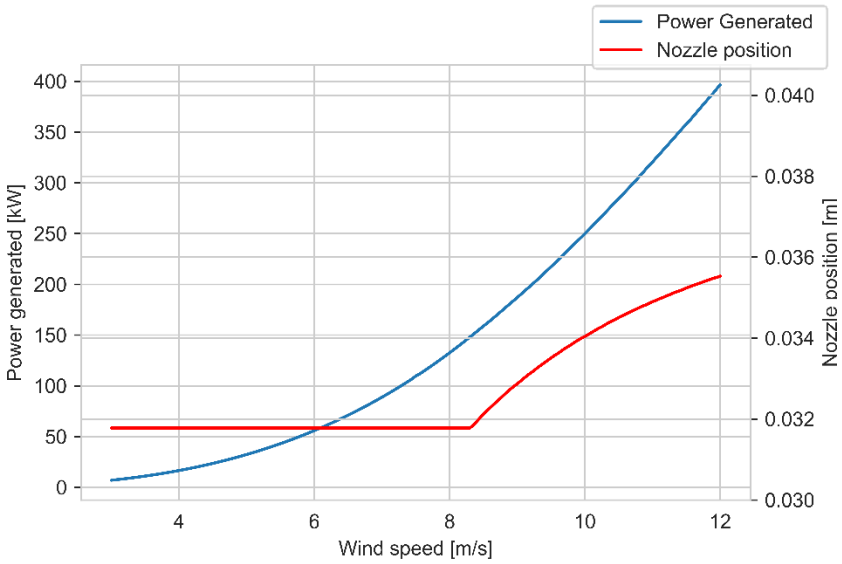

Figure 5. 2 Power generated and corresponding nozzle position for maximum electricity production.

The power generated by the DOT system is plotted on the left Y-axis and the subsequent nozzle position is plotted as a function of wind speed on the right Y-axis. It can be observed from the graph above, that the nozzle position remains constant for wind speeds up to 8.29 m/s. Hence up to 8.29 m/s, the DOT500 turbine operates on the K_{opt} control curve. This is the wind speed at which the Kamat high-pressure pump flow limit is reached. Since a positive displacement hydraulic pump is coupled to the high-speed shaft of the hydraulic drive train and the flow rate of the pump is directly proportional to the rotational speed of the high-speed shaft, the rotational speed of the turbine has to be maintained constant to maintain the flow rate of the high-pressure pump below its maximum limit. Hence, only the torque of the DOT500 turbine can be increased to maximize the power generated by the pelton. This leads to the movement of the nozzle towards close position, decreasing its effective area to increase the pressure in the system and, consequently, lead to an increase in torque generated on the pelton wheel. A small drop in the slope of the power generated curve occurs at 8.29 m/s, because the turbine rotational speed is no longer increasing linearly with the wind speed, the rotor no longer operates on its maximum performance. The maximum power generated by the system is 398 kW and hence for this mode of operation, 79.6% of the DOT500 turbine's rated power before the high-pressure pump can be realized. This reduction of 20% of power generated is due to several factors. Firstly, there is a reduction in turbine performance by operating the turbine at rotational speeds lower than the optimum. The losses of various system components are accounted for between the turbine and output of the pelton turbine. Lastly, the rated wind speed of the turbine could actually be a bit higher than 12 m/s.

The feed seawater pressure as a consequence of the nozzle position and the rotational speed of the high-pressure pump at different wind speeds is shown in Figure 5.3 below:

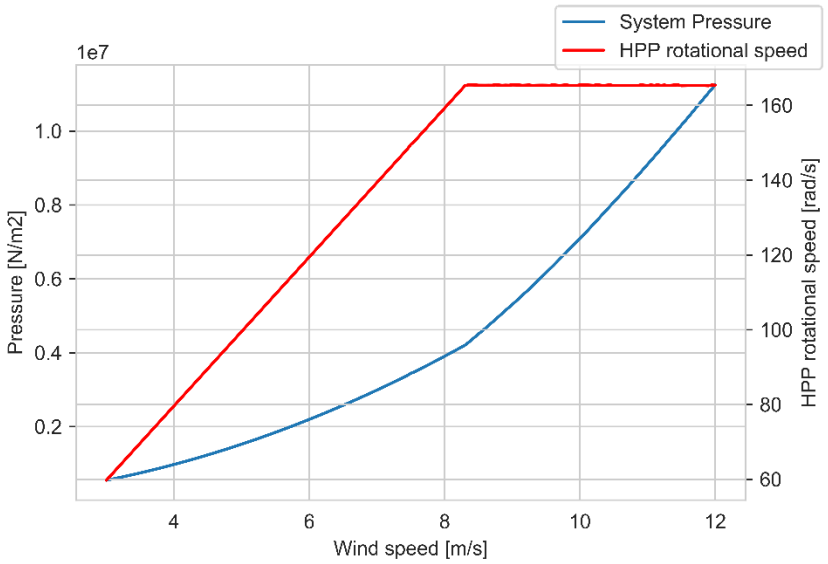

Figure 5. 3 System pressure and rotational speed of the high-pressure pump for maximum electricity production.

Since the flow rate limit of the high-pressure pump is reached at 8.29 m/s, the rotational speed of the rotor has to be maintained constant. Hence to maximize the power generated in the pelton turbine, the torque has to be increased. This results in the slope of the pressure curve to increase at 8.29 m/s.

The torque and rotational speed generated in the pelton turbine wheel as a consequence of the high-pressure jet of water impinging on it is plotted in Figure 5.4 below:

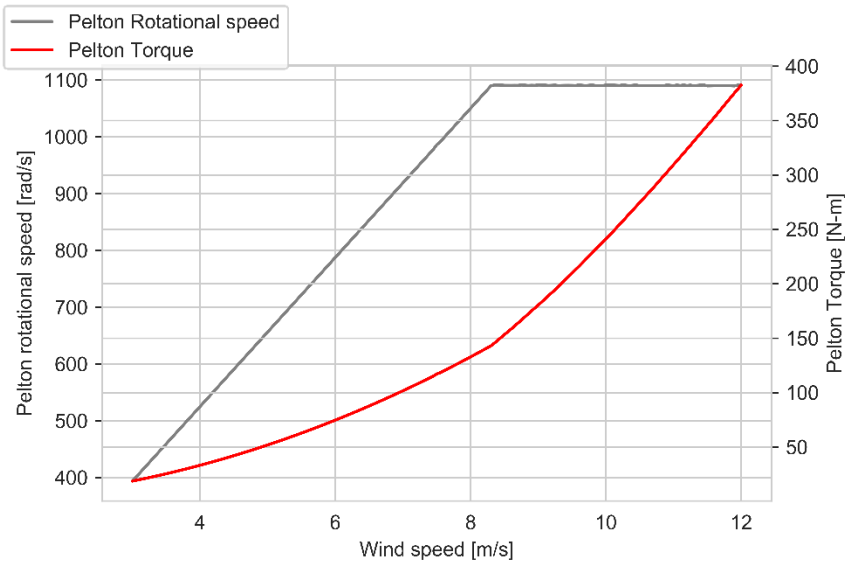

Figure 5. 4 Torque and rotational speed of pelton turbine for maximum electricity production.

Up to the wind speed of 8.29 m/s, the rotational speed of the pelton wheel, indicated in grey, exhibits linear behavior, similar to the linear behavior of the high-pressure flow rate. This proves that the valve of the RO is closed and all the flow from the high-pressure pump impinges onto the pelton turbine wheel. At 8.29 m/s, the slope of the torque generated in the turbine indicated in red increases, indicating the operation of the high-pressure pump at its flow limit.

The power consumed by the entire system is constant for all wind speeds and is equal to the power consumed by the boost pump and the sensors. It is negligible when compared to the power generated by the system.

5.2 Optimization for maximum water production

Optimization of the system for maximum water production is performed by an algorithm written in Python. This algorithm first uses the algorithm described in chapter 3 to solve for the system of flow equations. The pressure in the system, p for all wind speeds and nozzle positions are first obtained and the flow through the nozzle, Q_{nz} is calculated for all pressures. The high-pressure pump flow to the RO unit, $Q_{f,HPP}$ is calculated for pressures above osmotic pressure.

The minimum wind speed at which the osmotic pressure can be reached at any given nozzle position is first obtained, as this is independent of the permeability coefficient, K_w. This wind speed can be referred to as 'U_{osm}'. To detect U_{osm}, the algorithm looks for the position of the nozzle at which the turbine can operate at the maximum possible torque at the lowest wind speed. For wind speeds below U_{osm}, the system is optimized for maximum electricity production, since pressures above osmotic pressure cannot be reached and hence feed water cannot be desalinated. The turbine operates on the maximum coefficient of power, C_p and its corresponding tip speed ratio. Since for wind speeds above U_{osm}, the volume of permeate produced is directly proportional to the pressure above osmotic pressure, the algorithm looks for the nozzle position at which the system can operate at the maximum possible pressure. For all wind speeds, the algorithm checks if the pressure limit of the membrane, maximum permeate flow limit and the high-pressure pump flow/rotational limits are exceeded and chooses the position of the nozzle at which maximum pressure can be reached satisfying all the above-mentioned limits.

The torque and rotational speed of the DOT500 rotor operation when optimized for maximum water production is shown in Figure 5.5 below:

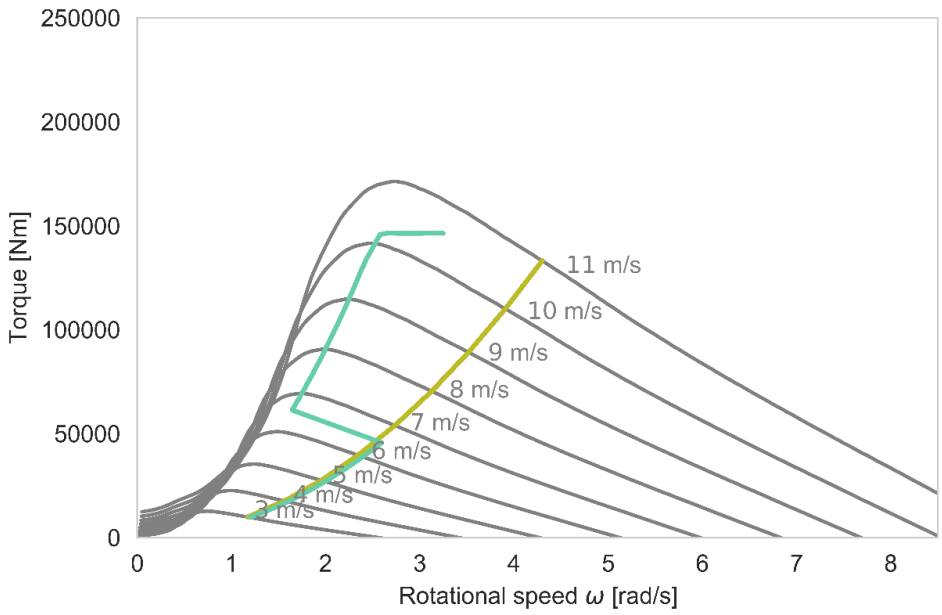

Figure 5. 5 Control curve of the DOT500 turbine for maximum water production.

The grey curves shown in Figure 5.5 above indicate the aerodynamic torque-rotational speed relationship for different wind speeds. The yellow curve is the operation of the wind turbine at maximum power coefficient for maximum power extraction from the wind. The aqua blue curve represents the operation of the turbine for optimization of maximum water production. It can be observed that up to U_{osm}, the operating curve overlaps the K_{opt} curve indicating that the system is operating to maximize the power extracted from the wind and hence maximum power is generated using the pelton turbine. At U_{osm}, the algorithm looks for the nozzle position at which the torque in the rotor at the respective wind speed is the maximum. Therefore at 6.54 m/s, the torque increases radically from τ_{opt} to the torque corresponding to a pressure above osmotic pressure causing the system to operate at a lower rotational speed, hence lower flow of the high-pressure pump. From U_{osm} to the wind speed at which the maximum allowable membrane pressure limit is reached at 10.29 m/s, the turbine operates at the peak of the torque-rotational speed curves to maximize the torque and pressure and hence produce the maximum possible amount of water at the respective wind speeds. At the wind speed at which one of the system limits is reached, the maximum allowable membrane pressure in this case, the system operates to keep the torque constant by opening the spear valve. This results in the constant operation of the RO system at the maximum pressure limit with constant feed flow to the membranes. To maximize the revenue generated by the DOT system, from 10.29 m/s, the rotational speed of the DOT500 turbine is increased while maintaining the rotor torque at the maximum membrane pressure limit. This results in the increase of flow from the high-pressure pump to the pelton turbine via the nozzle, thereby, increasing the power generated by the pelton turbine. At 10.45 m/s, the high-pressure pump flow limit is reached. To maintain constant water production in full load conditions, without damaging the high-pressure pump and the RO membranes, the flow and pressure has to be maintained constant by pitching. Thus, the blades of the DOT500 turbine needs to be pitched to operate the turbine at a constant rotational speed and constant torque, to continue production of water at constant preferable conditions for wind speeds above 10.45 m/s. The cut-out wind speed is therefore reduced from 12 m/s to 10.45 m/s and pitching of the blades occurs at a lower wind speed. The operation of the turbine in the unsteady region is avoided as a consequence of this optimization.

The pressure in the system for maximizing water production and the position of the nozzle is shown in the Figure 5.6 below:

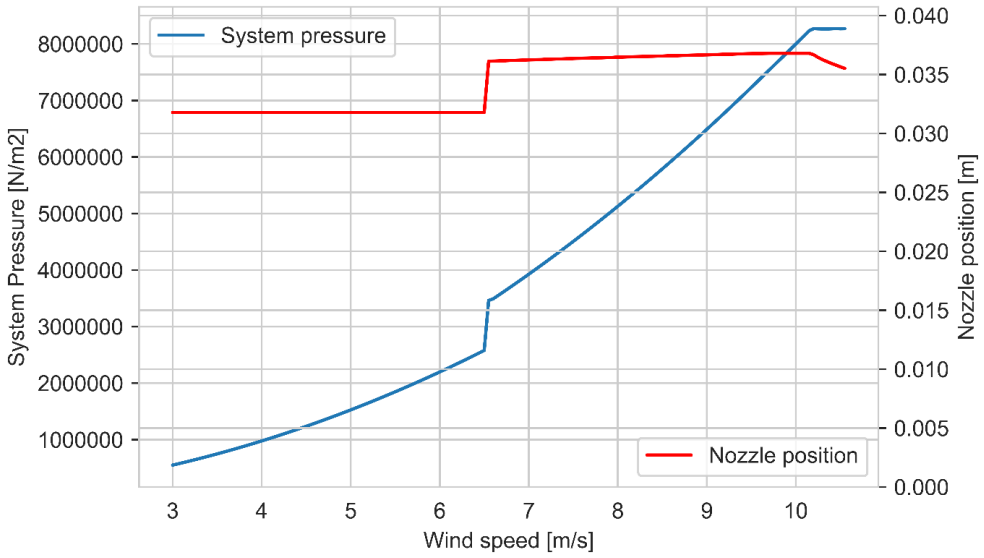

Figure 5. 6 System pressure and nozzle position for maximum water production.

For wind speeds below U_{osm} equal to 6.54 m/s, the valve of the RO remains closed and the system operation is the same as in the previous case. At $U_{osm,}$ it is possible to reach a pressure value just above osmotic pressure and hence the nozzle moves towards close position leading to a jump in the pressure of feed seawater from 25 bar to 34 bar to start reverse osmosis as seen in the blue curve in Figure 5.6 above. As the wind speed increases, the nozzle in the spear valve further closes to operate at the highest possible pressure at the corresponding wind speed. At 10.29 m/s, the pressure limit of the membranes is reached and hence the nozzle opens to maintain the pressure close to the membrane pressure limit of 82.7 bar, thus maximizing the production of water for wind speeds above U_{osm}. At 10.45 m/s, the flow rate limit of the high-pressure pump is reached. To maintain the system pressure at the limit, to prevent damage to the RO membranes, the torque of the DOT500 rotor is not allowed to increase further. Since the goal of this optimization is to maximize for water production, the blades of the DOT500 have to be pitched to maintain operation at constant rotational speed and torque. Hence the rated wind speed, U_{rated} is reduced to 10.45 m/s and is discussed in detail when analyzing the control curve of the turbine rotor above.

The torque and rotational speed of the pelton turbine are shown in the Figure 5.7 below:

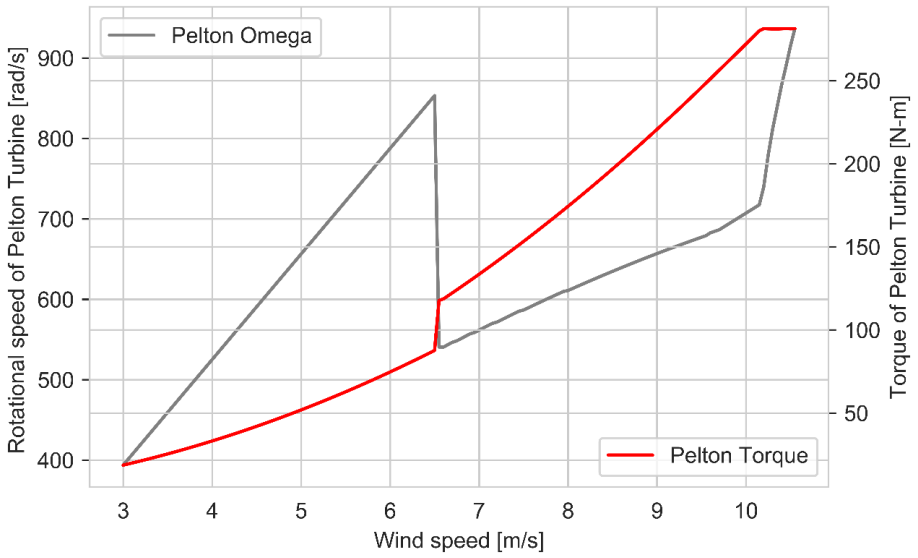

Figure 5. 7 Torque and rotational speed of the Pelton turbine for maximum water production.

The rotational speed generated in the pelton turbine indicated in grey exhibits linear behavior for wind speeds up to U_{osm} as discussed in the optimization for maximum electricity production case. Since the production of water starts at U_{osm}, a drop in the rotational speed generated in the pelton turbine is observed. This is due to the drop in the flow of feed from the high-pressure pump through the nozzle which is deviated towards the RO system. Since the pressure in the system jumps from 25 to 34 bar at U_{osm}, a proportional rise in the torque generated is visible.

The rotational speed of the high-pressure pump has similar characteristics in shape to the rotational speed curve of the pelton turbine but lower values due to the higher volumetric displacement of the pump compared to that of the pelton turbine.

The flow rate of freshwater produced, and amount of electricity generated by the system when optimized for maximum water production are shown in Figure 5.8 below:

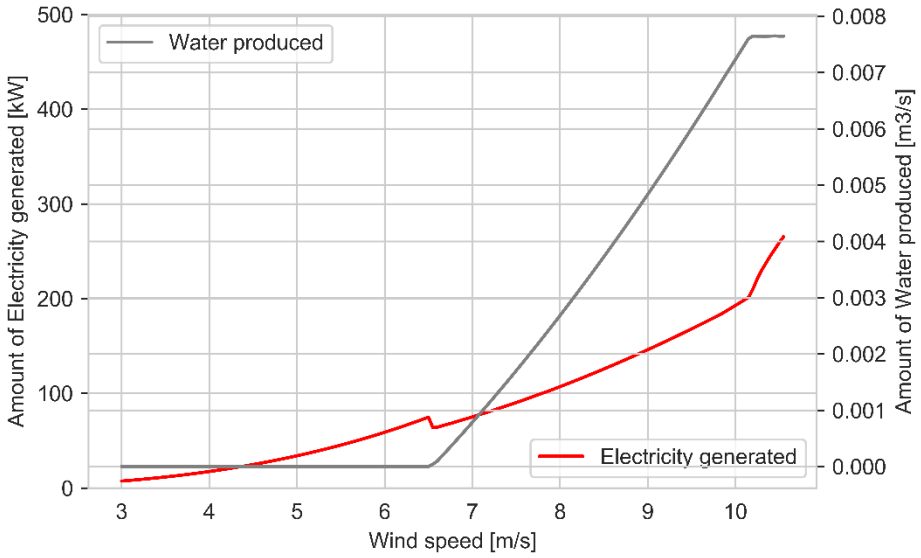

Figure 5. 8 Flow rate of permeate produced and amount of electricity generated for maximum water production.

The grey curve represents the flow rate of permeate produced as a result of desalination of seawater from reverse osmosis in m^3/s and the red curve represents the power generated by the pelton turbine generated in kW. The production of water begins at U_{osm} and below this wind speed, no permeate is produced. All the energy extracted from the wind is utilized to generate electricity by operating the turbine at maximum power coefficient. At U_{osm}, a drop in the power generated is seen because part of the feed water is diverted from the high-pressure pump to the RO proportionally to the excess pressure above osmotic pressure. Even though there is a rise in the torque of the rotor to increase the pressure above osmotic pressure to accommodate the start of reverse osmosis by closing of the nozzle, the flow through the nozzle reduces drastically and hence the rotational speed generated in the pelton wheel is reduced. Figure 5.6 shows that the pressure limit of the membrane is reached at 10.29 m/s and hence the pressure in the system is maintained constant resulting in the constant production of water. An increase in the power generation is seen at 10.29 m/s since the pressure limits the further increase in water production. The remaining flow from the high-pressure flow is diverted towards the pelton turbine resulting in the increase of rotational speed generated on the pelton wheel shaft at this wind speed. The flow rate through the ERD and its rotational speed have similar characteristics in shape as the grey curve in Figure 5.8 above.

The power consumed by the entire system when optimized for maximum water production shows similarity in shape as the red curve in Figure 4.6. Since the ERD starts operating at 6.54 m/s instead of 7.5 m/s, the increase in power consumption is visible at this wind speed and the drop in the consumption curve visible at 11.6 m/s is absent. Hence, above 11.6 m/s, less power can be delivered to the grid compared to operation on the turbine maximum power curve.

5.3 Optimization for specified locations

Optimization for maximum electricity production and maximum water production is performed for 3 locations namely:

1. Maasvlakte, within the Port of Rotterdam, The Netherlands having coordinates (Lat, Long): (51.97156°, 4.01379°) marked in the map in Figure 5.9 below:

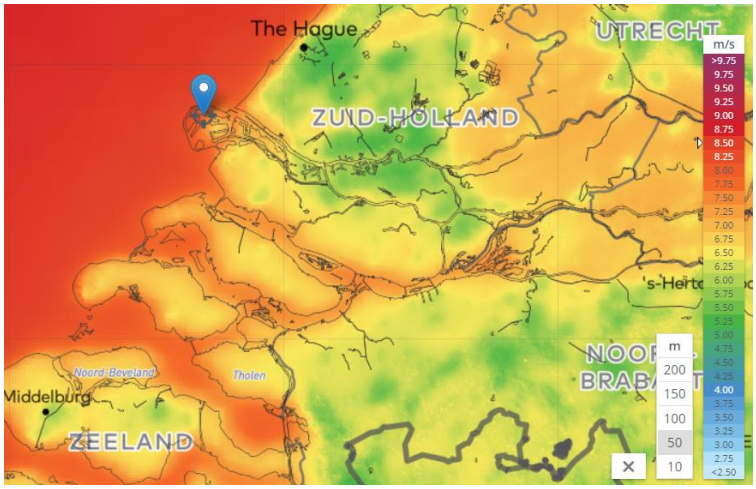

Figure 5. 9 Location 1 : Maasvlakte [23].

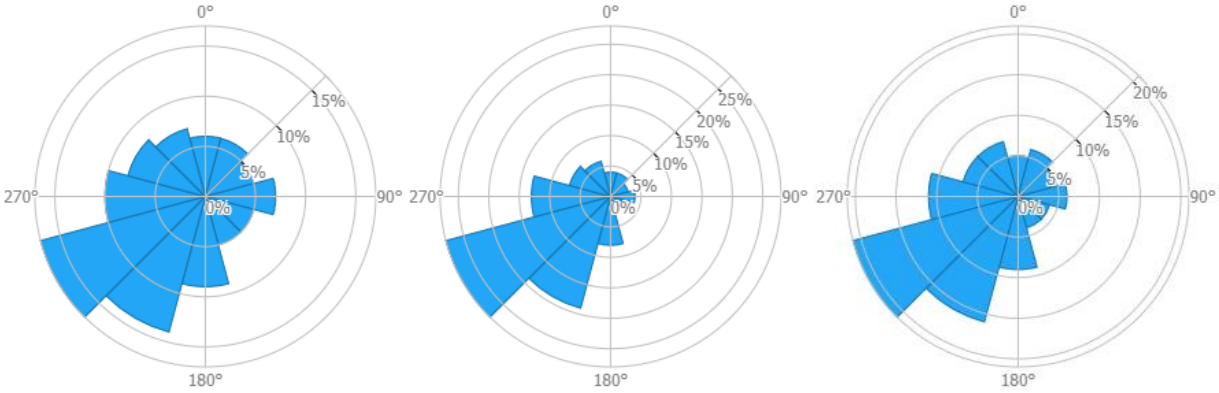

Figure 5. 10 Wind frequency rose (left), Wind power rose (middle) and Wind speed rose(right) for Maasvlakte [23].

The wind frequency rose (left), wind power rose (middle) and the wind speed rose for Maasvlakte is obtained from global wind atlas and is shown in Figure 5.10 above. From the wind rose diagram it can be concluded that the dominant winds comes from the south-west direction for Maasvlakte. The mean power density is 635 W/m^2 and the average wind speed is 8.19 m/s.

2. Aruba (North), in the southern Caribbean Sea having coordinates (Lat, Long): (12.56763 $^\circ$, -69.99699 $^\circ$) is marked in the map in Figure 5.11 below:

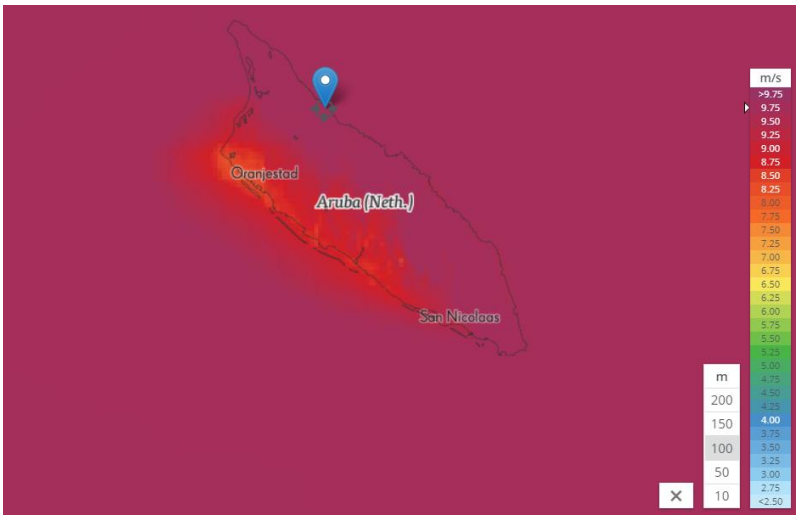

Figure 5. 11 Location 2 : Aruba North [23].

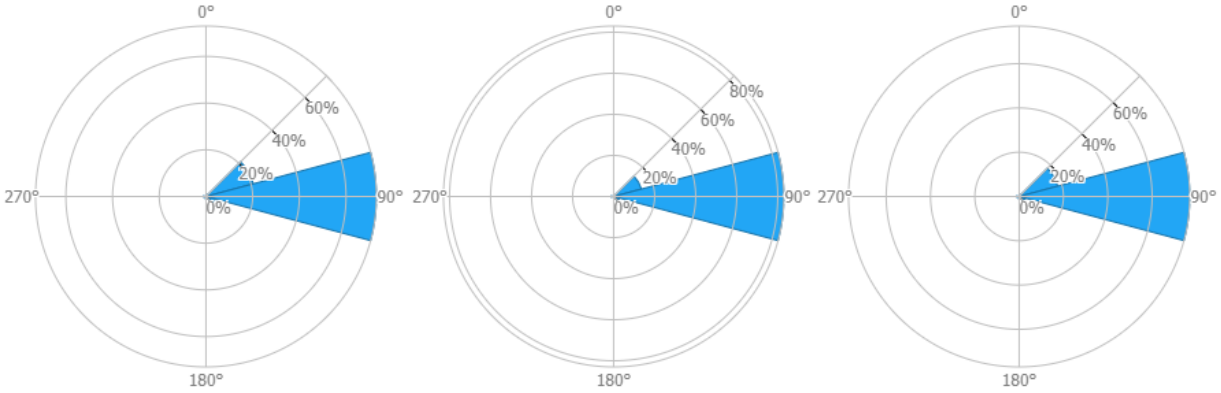

Figure 5. 12 Wind frequency rose (left), Wind power rose (middle) and Wind speed rose(right) for Aruba North [23].

The wind frequency rose (left), wind power rose (middle) and the wind speed rose (right) for Aruba South is shown in Figure 5.12 above. 90% of the dominant winds are eastern for Aruba north. The location has a mean power density of 909 W/m^2 and average wind speed of 10.93 m/s.

3. Aruba (South) having coordinates (Lat, Long): (12.47748 $^\circ$, -69.99463 $^\circ$) is marked in the map in Figure 5.13 below:

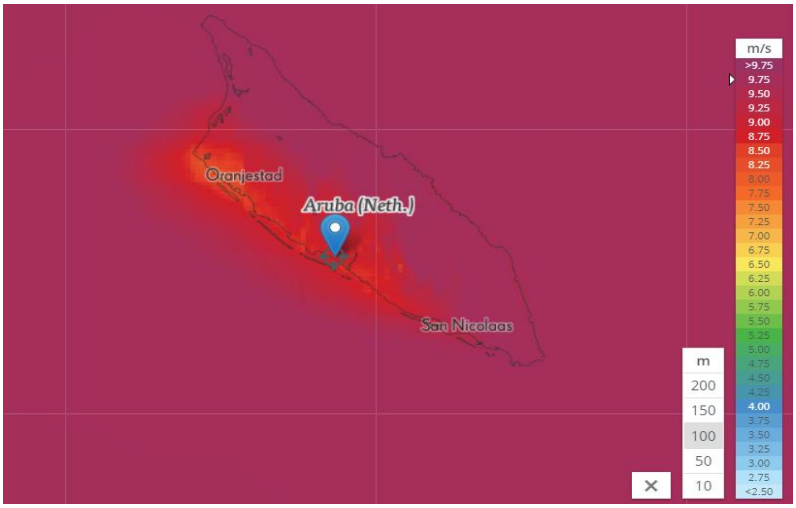

Figure 5. 13 Location 3 : Aruba South [23].

This particular installation site located in the South of Aruba has the exact same wind frequency rose, wind power rose and wind speed rose as Aruba North shown in Figure 5.12 and hence the dominant winds blow from the east direction. The mean power density is 529 W/m^2 and average wind speed is 9.18 m/s.

The wind speed distribution of all the 3 locations is shown graphically using the Weibull distribution curve in Figure 5.14 below:

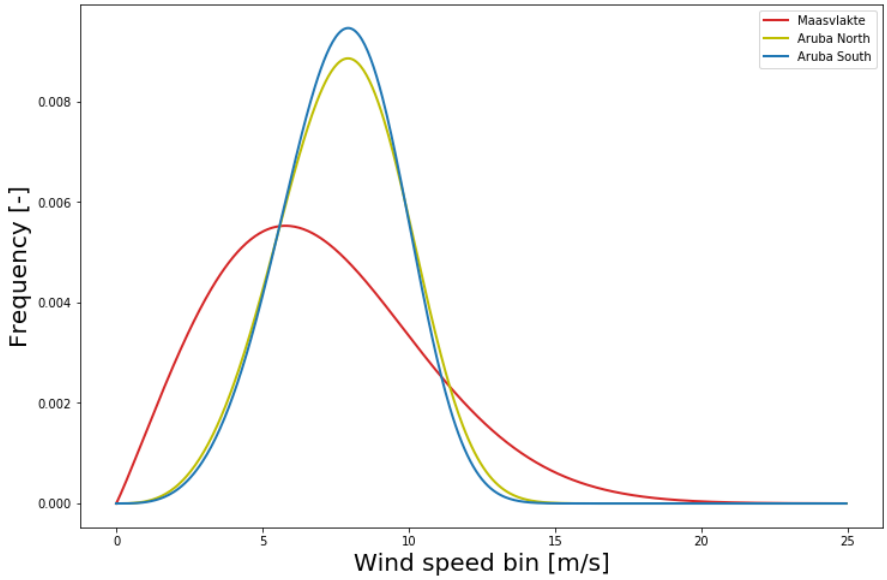

Figure 5. 14 Weibull distribution of Maasvlakte, Aruba North and Aruba South.

The data is sorted into wind speed classes of 0.05 m/s. The Weibull scale parameter 'A' [m/s] is a measure for the characteristic wind speed of the distribution for the particular location. The Weibull scale parameter is also proportional to the mean wind speed. The Weibull shape parameter 'k' is a measure of the shape of the wind speed distribution. Smaller the value of k, more the variation in wind speeds. Both these Weibull parameters for all 3 locations are calculated and defined in Table 5.2 below.

Table 5. 2: Weibull parameters for the 3 specified locations.

Location	Scale parameter 'A' (m/s)	Shape parameter 'k'
Maasvlakte	7.95	2.073
Aruba North	8.52	3.965
Aruba South	8.45	4.216

The revenue from water production and electricity generation is plotted for all 3 locations for optimization of the system for maximum electricity production and maximum water production. Using the frequency of distribution of wind speeds from Weibull distribution curve, the occurrence of all wind speeds in 0.05 m/s bins in number of hours per year is calculated from cut-in to cut-out wind speeds. A realistic fixed price for cubic meter of water and kilowatt-hour of electricity, as shown in Table 5.3 below, is assumed and the revenues for every wind speed are calculated.

Table 5. 3: Selling price of water and electricity for the 3 specified locations [24] [25].

Location	Price of 1m^3 of water [€]	Price of 1kWh of electricity [€]
Maasvlakte	1.04	0.05
Aruba North	4.06	0.25
Aruba South	4.06	0.25

The total annual energy produced at every wind speed, U is calculated by multiplying the power generated at the respective wind speed, P(U) with the number of hours in a year at the particular wind speed, t(U) obtained from the Weibull distribution as shown in Equation 5.1.

$$E(U) = P(U) \cdot t(U) \tag{5.1}$$

5.3.1 Revenue from optimization for maximum *electricity* production:

The product of total annual energy produced, E(U) and price of electricity in euros per kilowatt-hour gives the annual revenue in euros from system operation at corresponding wind speeds.

The revenues from production of electricity and water for Maasvlakte, Aruba north and Aruba south are shown in Figures 5.15, 5.16 and 5.17 below.

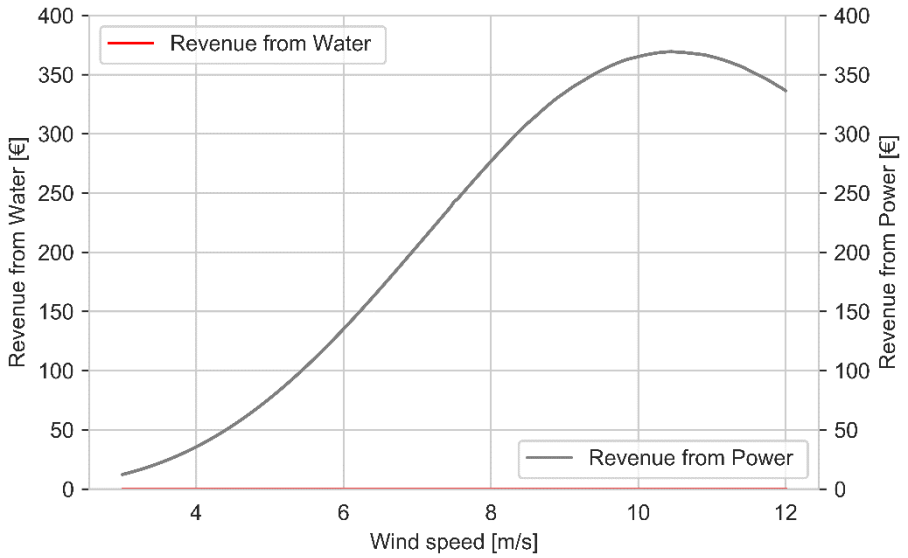

*Figure 5. 15 Revenue from electricity production at **Maasvlakte.***

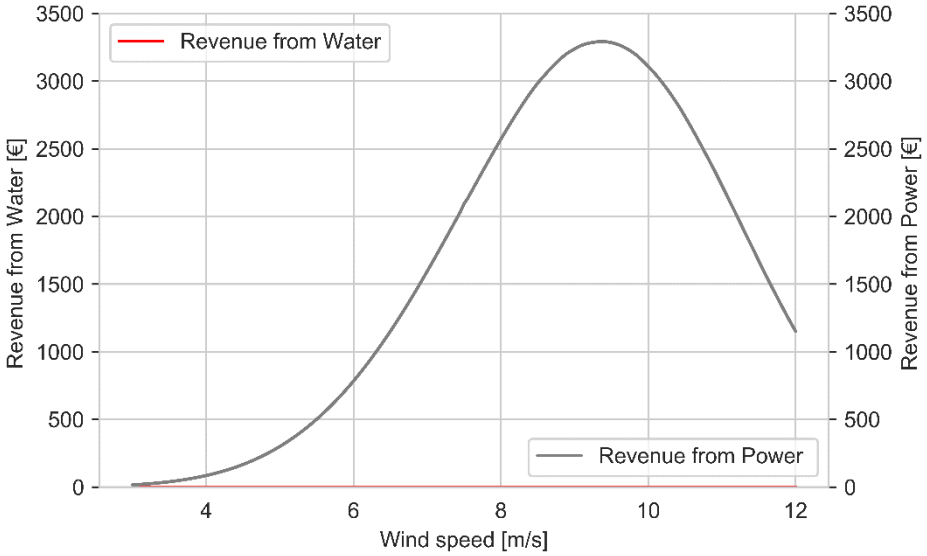

*Figure 5. 16 Revenue from electricity production at **Aruba North.***

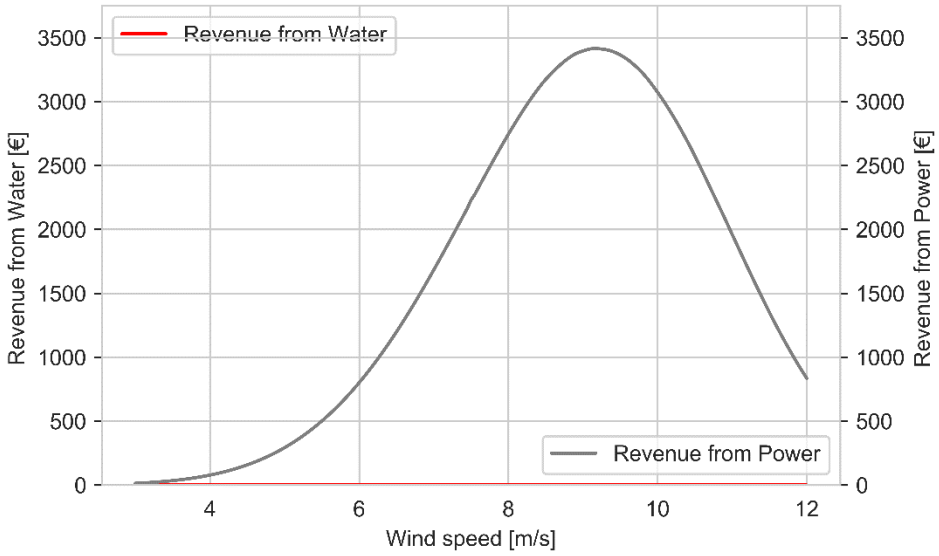

*Figure 5. 17 Revenue from electricity production at **Aruba South.***

The revenue from electricity production for a year in Euros is represented by the gray curve in the figure above. The revenue from water production in red is 0 for all wind speeds because the RO valve is closed to maximize electricity production.

5.3.2 Revenue from optimization for maximum *water* production:

The total flow rate of water produced in a year for every wind speed, U is calculated by multiplying the flow rate of water produced at every wind speed, $Q_p(U)$ shown in Figure 5.8, translated to m^3/hour, with the number of hours in a year at the particular wind speed, t(U) obtained from the Weibull distribution. This is shown in Equation 5.2 below:

$$Q_{p,year}(U) = Q_p(U) \cdot t(U) \qquad (5.2)$$

The product of the annual volume of the water produced at every wind speed, $Q_{p,year}$ and the price per cubic meter of water at the particular location in Euros defined in Table 5.3 gives the annual revenue from water production by the DOT system at corresponding wind speeds.

The revenues from production of electricity and water for Maasvlakte, Aruba north and Aruba south for a year in Euros are shown in Figure 5.18, 5.19 and 5.20 below:

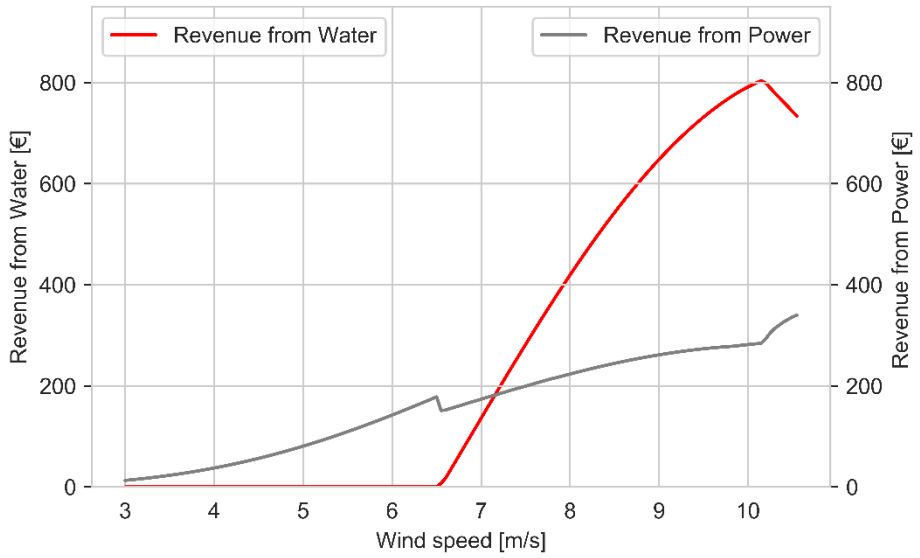

*Figure 5. 18 Revenue from electricity and water production at **Maasvlakte.***

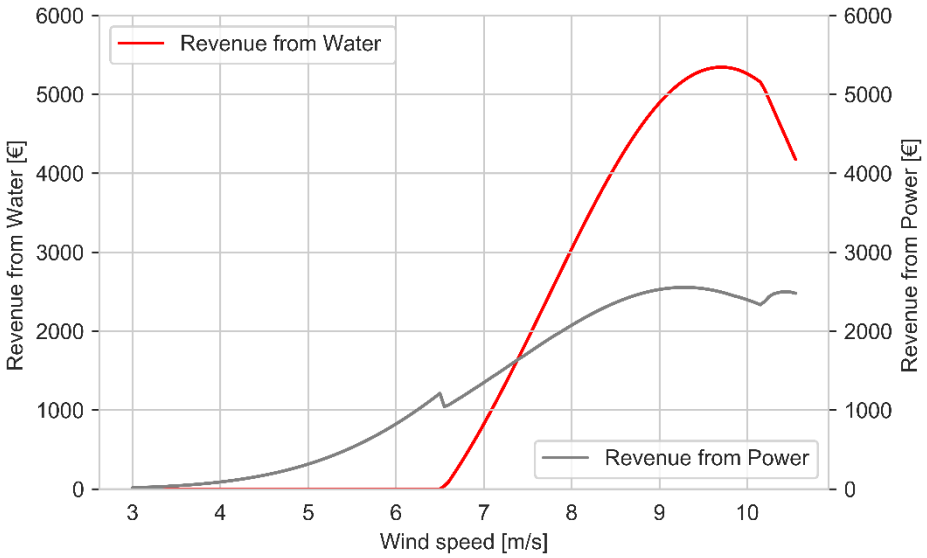

*Figure 5. 19 Revenue from electricity and water production at **Aruba North.***

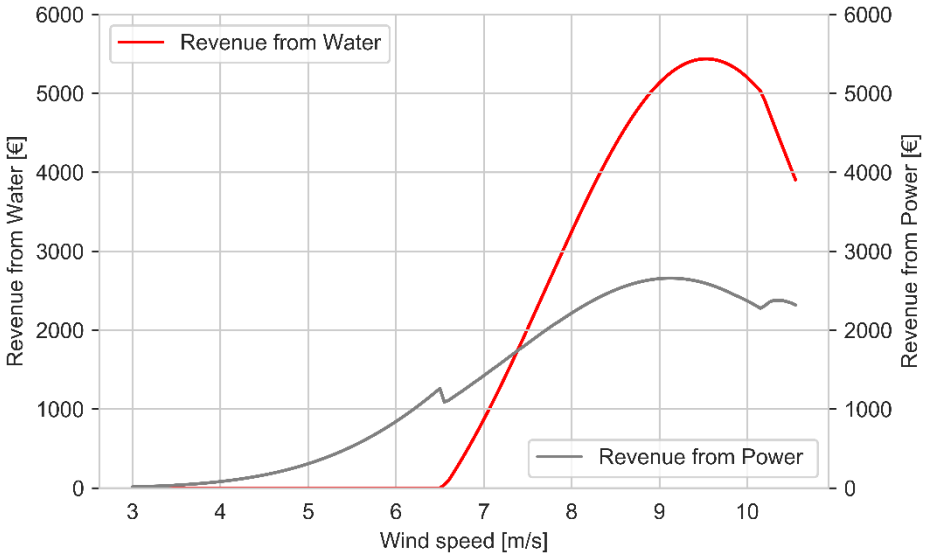

*Figure 5. 20 Revenue from electricity and water production at **Aruba South.***

The grey curves represent the revenue from electricity production for a year in Euros and the red curves represent the revenue from water production.

Chapter 6: Sensitivity Analysis

For the DOT system optimized for maximum water production in Chapter 5, the sensitivity of two independent desalination parameters, active membrane area of RO modules, 'A_m' and permeability coefficient, 'K_w', on dependent variables, like cut-out wind speed, maximum permeate production, maximum system operating pressure, power generated by the pelton turbine, total annual power and water produced, under a given set of assumptions, is analyzed in this chapter.

A few points of the sensitive parameters, referred to as knots, are chosen depending on the parameter within a realistic range of values and the simulations are run. The variables dependent on the sensitive parameters are noted. To predict the values that fall within the chosen points of sensitive parameters, nonlinear spline interpolation is performed using 'InterpolatedUnivariateSpline' function. Spline interpolation is chosen in order to draw a smooth curve through the chosen data points.

6.1 Sensitivity of membrane active area 'A_m'

The active area of the membrane is an important parameter which can be chosen while designing the system to calibrate the model according to the requirement of a particular location. To analyze the effect of A_m on various output parameters, the maximum water production optimization simulation is run for 5 Filmtec membranes having similar properties but varying in membrane active areas from 28m^2 to 41m^2.

The membranes chosen to perform sensitivity analysis of A_m is shown in Table 6.1 below.

Table 6. 1: Membranes chosen for sensitivity analysis of A_m.

Model	Active membrane area (m^2)
SW30-8040	28
SW30HR-320	30
SW30-380	35
SW30HR LE-400	37
SW30XLE-440i	41

All the other system parameters like permeability coefficient, maximum allowable membrane pressure, membrane permeate production limit, number of membranes and pressure vessels, high-pressure pump / pelton turbine type, flow, volumetric displacement and rpm limit, concentration of feed seawater, type of spear valve, membrane recovery rate and various volumetric and mechanical efficiencies are kept constant, as described in Table 4.1, to lay a basis for comparison.

By varying the active areas of membranes in the RO system, the rated wind speed for DOT500 turbine operation varies as shown in Figure 6.1 below.

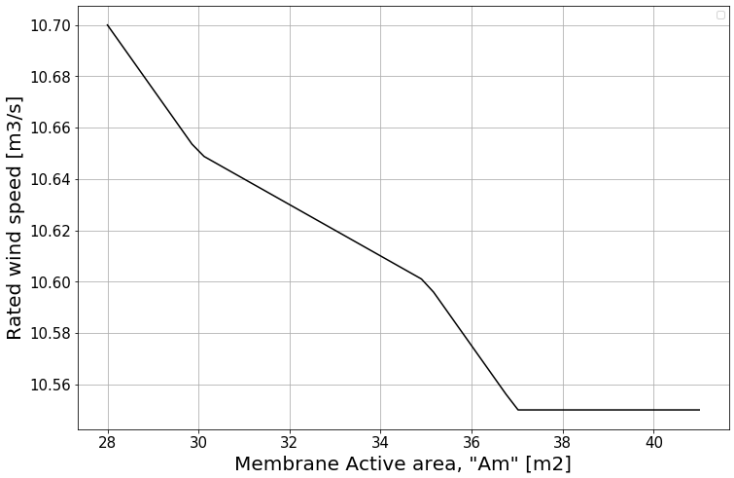

Figure 6. 1 Sensitivity of rated wind speed at different A_m.

The rated wind speed for this system can be defined at the wind speed at which both the torque and rotational speed limits are reached. An increase in the torque, would result in the increase in system pressure beyond the membrane pressure limit. Similarly, an increase in the rotational speed, would result in the exceedance of flow rate limit of the high-pressure pump. Thus, the blades have to be pitched at this rated wind speed, to maintain constant torque and rotational speed at the system limits, by turning the angle of attack of the blades according to pitch control.

It can be observed that as the size of the membrane active area increases, the rated wind speed decreases and hence, the blades of the turbine have to be pitched at lower wind speeds, to maintain constant production of water and power at the respective rated limit.

For the entire range of A_m, the system operation is limited by the maximum membrane allowable pressure to maintain maximum water production. As A_m increases, at higher wind speeds the turbine operates at the torque corresponding to pressure limit of the membrane but at higher rotational speed. Thus, for a lower membrane active area, the torque limit is reached at a lower rotational speed leaving larger room for the system operation at constant torque up to the rotational speed limit causing the rated wind speed to be higher. Similarly, for a higher value of A_m, the torque limit is reached at a higher rotational speed, thus the rated wind speed is lower, and the pitching of blades occurs at lower wind speeds.

The sensitivity of the minimum wind speed at which water can be produced at different A_m is shown in Figure 6.2 below. It can be observed that for all A_m between 28 to 41m^2, water production starts at a constant wind speed of 6.55 m/s. This is because the system is designed to find the minimum wind speed at which the torque is high enough to operate the system at pressures above osmotic pressure. This wind speed is independent of A_m, because the size of the membrane does not directly influence the operating point of the turbine. Thus, for all membrane sizes, the system can be designed to operate at $C_{p,max}$ to maintain operation on the maximum power production curve below 6.55 m/s.

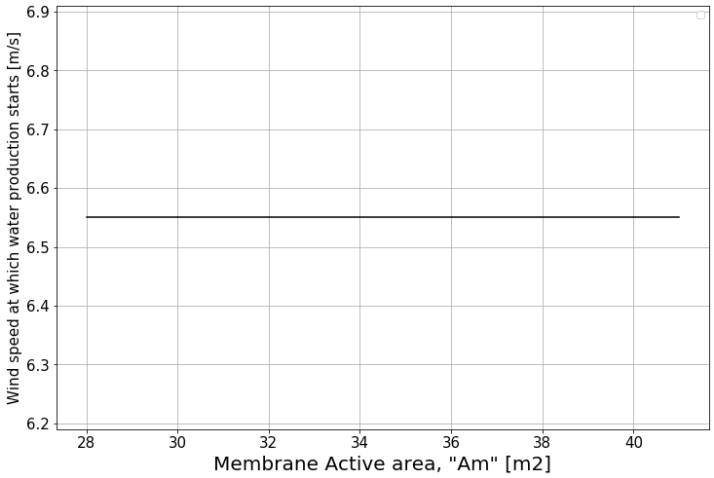

Figure 6. 2 Minimum wind speed at which water production starts for different A_m.

The maximum permeate flow rate at different A_m is shown in Figure 6.3 below.

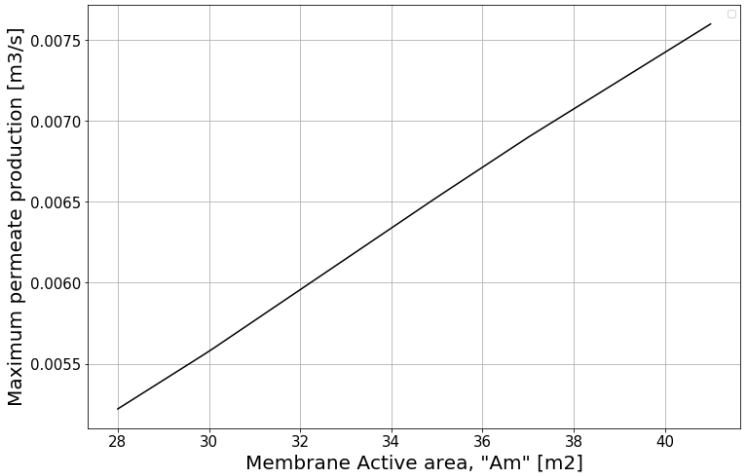

Figure 6. 3 Maximum permeate production at different A_m.

The flow rate of permeate produced is the membrane recovery rate, γ times the total feed flow to the RO system as defined in Equation 3.26. The total feed flow consists of the feed flow from the high-pressure pump and the feed from the ERD as defined in Equation 3.12. The feed flow from the high-pressure pump to the RO varies according to Equation 3.17, and is linearly proportional to the membrane active area, A_m. Thus, it can be concluded that the permeate production is linearly proportional to A_m. This relation can be seen in the figure above. The increase in membrane active area results in a linear increase in the maximum permeate produced by the RO unit. A slight deviation from the linear behavior is visible due to the selection of knots in irregular intervals within the range considered for this sensitivity study. Increasing the number of membranes in the system will exhibit similar behavior.

The pelton turbine characteristics for different A_m are plotted in Figure 6.4 below.

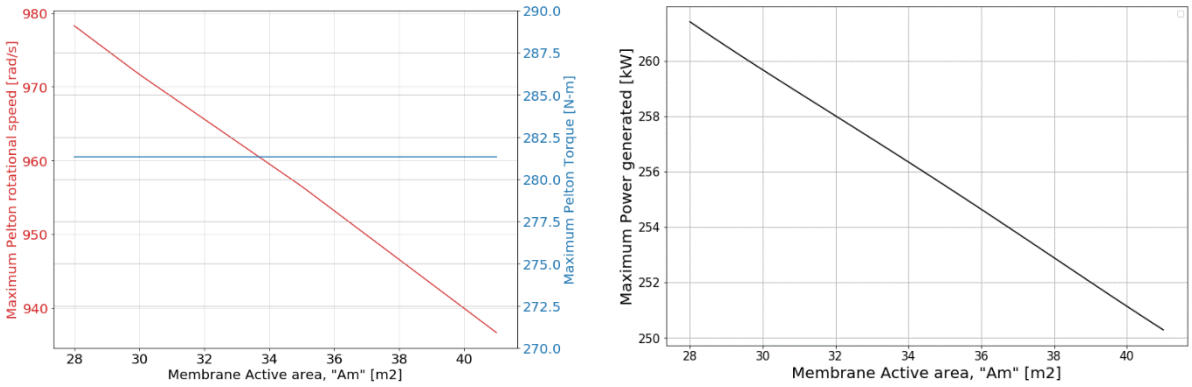

Figure 6. 4 Maximum pelton turbine torque and rotational speed generated at different A_m (left), Maximum power generated by the system at different A_m (right).

The red curve in Figure 6.4 (left) indicates the maximum rotational speed and the blue curve indicates the torque generated by the pelton turbine. Figure 6.4 (right) shows the maximum power generated by the pelton turbine at different values of A_m.

The maximum torque generated by the system is constant for all values of A_m as shown in blue in the figure 6.4(left) above. This is because for any membrane size, at wind speeds before the rated wind speed the system already operates at the maximum RO membrane pressure limit to maintain constant operation of the RO, thus producing the maximum possible water within all limits. The goal is to maintain turbine operation at this torque limit for all wind speeds up to cut-off wind speed by pitching the blades.

This reasoning is validated by Figure 6.5 below showing the maximum pressure in the system for different values of A_m.

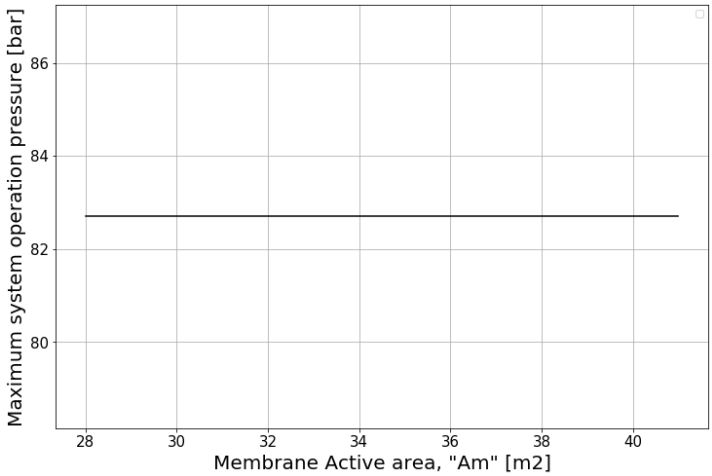

Figure 6. 5 Maximum system operating pressure at different A_m.

Figure 6.6 shows these wind speeds above which constant operation of RO is possible up to cut-out wind speed, i.e. 25 m/s.

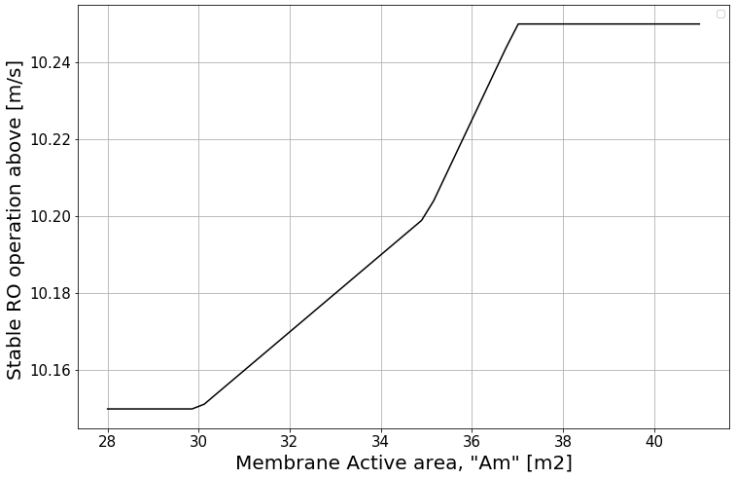

Figure 6. 6 Wind speeds above which constant RO operation is possible for different A_m.

Operation of the RO unit is most stable at constant pressures, and the main goal is to maximize water production i.e. operate at the membrane pressure limit. It can be observed from Figure 6.6 that as the active membrane area increases, the wind speed at which constant operation of the RO can be achieved also increases. This is because a decreasing trend in the rotational speed generated in the pelton turbine is seen in Figure 6.4(left). The rated wind speed keeps decreasing for an increasing A_m.

The RO feed flow from the high-pressure pump, $Q_{f,HPP}$ is linearly proportional to the membrane active area, A_m defined in Equation 3.17. Smaller the active membrane area, lower the high-pressure pump feed flow, $Q_{f,HPP}$ to the RO unit and therefore the constant operation of RO occurs at a lower wind speed. Hence higher the flow rate through the nozzle, Q_{nz}. Consequently, higher the rotational speed generated in the pelton turbine as seen in Figure 6.4 (left).

6.2 Sensitivity of permeability coefficient 'K_w'

The permeability coefficient has an impact on the efficiency of the desalination process [29]. This in turn has a significant effect on the various operating parameters of the DOT system. The permeability coefficient depends mainly on the material structure of the membrane. Nano-porous graphene and carbon nanotubes have permeabilities of 2-3 orders of magnitude higher than TFC membranes [29]. Hence, depending on the location, and electricity/water requirements, the type of membrane can be chosen. The implication of this choice has a substantial effect on process efficiency and permeate production by the reduction in operating hydraulic pressures.

To analyze the effect of K_w on various system output parameters, the simulation for optimization of maximum water production is run for 10 realistic values of K_w between $4.16 \cdot 10^{-8}$ to $4.16 \cdot 10^{-10}$ s/m [29]. All other system parameters mentioned in the sensitivity study of A_m, including the membrane active area from Table 4.1 are kept constant for comparison.

The variation of rated wind speed for the DOT500 turbine at different increasing values of K_w are shown in Figure 6.7 below:

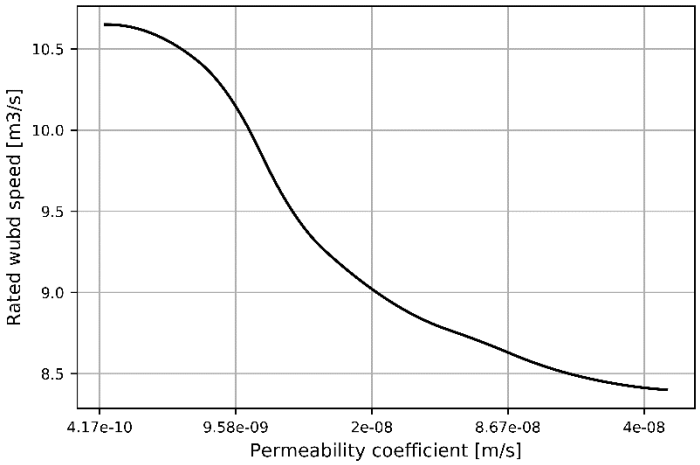

Figure 6. 7 Sensitivity of rated wind speed at different K_w.

The rated wind speed of the DOT500 turbine decreases with increasing permeability coefficient of the membrane. This is because, higher the permeability coefficient, lower the pressure required to produce the same flow rate of the permeate. Therefore, at higher values of K_w, the maximum allowable membrane pressure limit is reached at lower wind speeds and vice versa. The torque of the wind turbine has to be kept constant at this limit to avoid damage to the membranes, and hence the turbine can only operate at increasing rotational speeds for increase in wind speeds up to the high-pressure pump flow limit.

The minimum wind speed at which the production of water can start at different permeability coefficients is plotted in Figure 6.8 below:

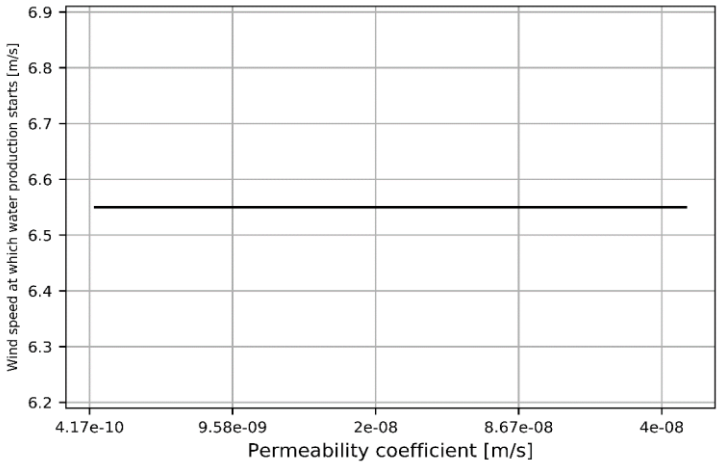

Figure 6. 8 Minimum wind speed at which water production starts for different K_w.

It can be observed from the above figure, that for all values of K_w, the minimum wind speed at which water can be produced remains independent of K_w. The value of permeability coefficient does not influence the operation of the turbine and hence has no effect on the pressure in the system. It mainly influences the volume of permeate produced at this wind speed. Lower the K_w, lower the permeate produced at this minimum wind speed and vice versa.

The maximum permeate flow rate at different K_w is shown in Figure 6.9 below.

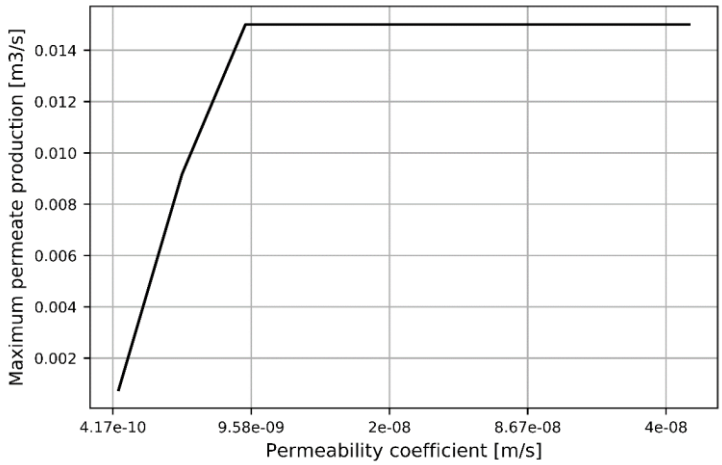

Figure 6. 9 Maximum permeate at different K_w.

The flow rate of permeate produced varies linearly with the permeability coefficient according to Equation 3.15. This linear behavior is visible for the lower spectrum of permeability coefficients considered for this study. Above a particular value of K_w, the maximum permeate produced by the RO system remains constant. This is due to the maximum permeate production limit of the entire RO system. Without this limit, the linear behavior is expected. The wind speed at which this maximum permeate production limit can be reached decreases for increasing K_w and is shown in Figure 6.10 below.

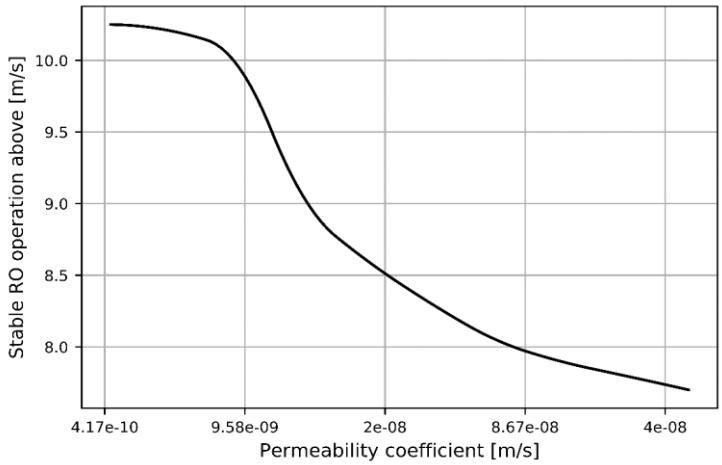

Figure 6. 10 Wind speeds above which constant RO operation is possible for different K_w.

The graph above represents the wind speeds at which the system operates at the membrane pressure limit for maximum water production. For low values of permeability coefficient, to operate the RO unit at its corresponding maximum permeate production limit, the system needs to operate at higher pressures. These high pressures can be reached only at higher wind speeds. As the K_w value increases, the RO unit can produce maximum water at its permeate limit (seen in figure 6.9), at pressures below the maximum allowable membrane pressure. Hence, these low pressures can be reached at lower wind speeds, leading to constant RO operation for a larger range of wind speeds.

The characteristics of the pelton turbine for different K_w are plotted in Figure 6.11 below.

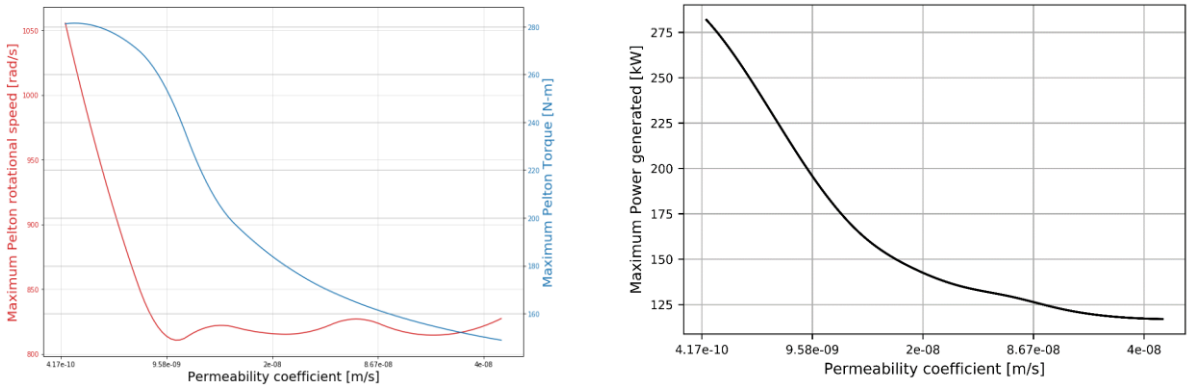

Figure 6. 11 Maximum pelton turbine torque and rotational speed generated at different K_w (left), Maximum power generated by the system at different K_w (right).

The red curve in the left figure above represents the maximum rotational speed and the blue curve represents the maximum torque generated by the pelton turbine. Figure 6.10 (right) indicates the maximum power generated by the system at different permeability coefficients.

As the permeability coefficient of the membrane increases, the torque generated by the pelton turbine decreases. This is because for increasing values of K_w, the maximum pressure at which the system operates also decreases, as the system operation is limited by the maximum permeate production flow rate of the entire RO unit at lower pressures. This is validated by Figure 6.12 below, where the maximum system operation pressure for increasing permeability coefficients is plotted.

The maximum rotational speed generated by the pelton turbine decreases for low permeability coefficients where the RO unit produces water below its maximum permeate production limit. This is because for low values of K_w, the flow from the high-pressure pump to the RO unit is higher to maximize water production and hence lower flow impinges on the turbine leading to a decrease in rotational speed generated. For the range of permeability coefficients where the permeate production limit is reached, (above $9.42 \cdot 10^{-9}$ s/m), the maximum rotational speed generated by the pelton turbine dips and rises due to the combination of decreasing turbine rated-wind speed and the flow rate through the nozzle. The maximum power generated by the turbine is a product of pelton torque and rotational speed.

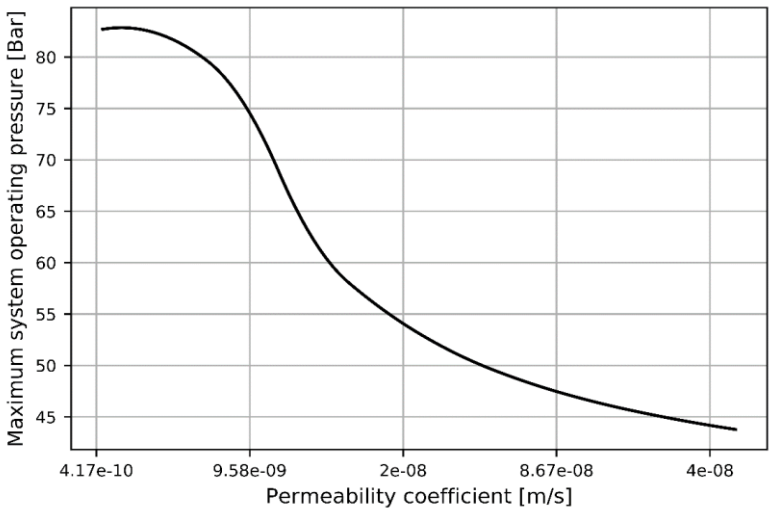

Figure 6. 12 Maximum system operating pressure for different K_w.

Chapter 7: Conclusions and Recommendations

The goal of this thesis was to investigate the steady-state performance of the wind powered freshwater and electricity production system, by controlling only the nozzle of the spear valve. A numerical model of a DOT500 hydraulic drive train wind turbine integrated with a RO system with ERD and a pelton turbine in parallel to the RO was made. The ultimate goal was to maximize revenue for specified locations by means of quantitative numerical modeling of the integrated system and simulation of the model for various scenarios. Optimization was performed for maximum water production and maximum electricity production using algorithms built and sensitivity analysis of critical desalination parameters was performed to investigate their effect on overall system performance.

7.1 Main Conclusions

The DOT hydraulic drive train turbine integrated to a RO with ERD for desalination and pelton turbine to generate electricity could be the solution to coastal developing countries where fresh water is scarcer and electricity is generated using conventional methods. The steady-state simulation of the model shows promising results in controlling the system with only a spear valve at fluctuating wind speeds up to rated wind speed.

The main research question was formulated in Chapter 1 as:

How can the DOT500 hydraulic drive train wind turbine be used to produce fresh water and electricity using a spear valve as means to control and optimize the system?

The spear valve is an electronically actuated throttle which can be used to widen or narrow the outlet area of the orifice. In the system modeled, for steady control of the hydraulic drive train wind turbine, the counter torque provided by the high-pressure pump can be influenced by the position of the spear valve to achieve desired pressure levels. This translates to the character of the control curve of the DOT500 turbine. Hence, the system operation can be optimized to either produce maximum power by maintaining operation close to the K_{opt} maximum power curve or produce maximum water by operating close to maximum torque. The model also confirms the stable operation of the system at its sub-system limits by manipulating the position of the nozzle to maximize revenue.

The numerical model and algorithm built to solve the system of steady-state equations in Chapter 3 aid in simulating the integrated system for all combinations of operating conditions. This helps in gaining deeper understanding of the system behavior, especially in recognizing the problematic operating region where the turbine operates at low tip speed ratios at near fully-closed nozzle positions, resulting in the loss of performance. For the range of tip speed ratios, where the turbine can produce power from the wind, certain nozzle positions where the spear valve is near fully-closed position, lead to multiple solutions. A unique solution can be found when ignoring the turbine operation at low tip speed ratios. It can be concluded that, with the help of this steady state model, the control settings for steady state conditions of the turbine can be formulated. Thus, the problematic operating region can be avoided, increasing system reliability, by maintaining operation of all the sub-system components within its nominal range of operation.

When simulating the model for maximum turbine power, the torque and rotational speed follows a quadratic function. At low wind speeds, the system only generates power and operates at a constant nozzle position. Above osmotic pressure, water production starts by moving the nozzle slightly towards the close position and the volume of permeate produced increases proportionally with the increase in torque. The valve of the RO is shut-off at high torques above the membrane maximum limit to prevent damage to the membranes, resulting in a jump in electricity production and the nozzle comes back to its original constant position. A similar turbine control strategy is obtained when optimizing for maximum

electricity production. The valve of the RO remains closed for all wind speeds and the position of the nozzle remains constant for wind speeds up to which the high-pressure pump flow limit is reached. Above this wind speed, the nozzle moves towards close-position to maintain operation at constant rotational speed, up to the rated wind speed, thus maximizing electricity generated.

The system can be optimized to generate maximum revenue by optimizing for maximum water production. The strategy is by closing the RO valve and operating the turbine on the maximum power curve for low wind speeds up to U_{osm}, which is the minimum wind speed at which the system can operate above osmotic pressures. Above U_{osm}, the optimum operating curve is as steep as possible, close to maximum torque, to maintain operation at the maximum possible pressure, maximizing production of water. When the membrane pressure limit is reached, the nozzle is opened to maintain the pressure at its maximum limit. This leads to constant production of water at the RO limit, while an increase in rotational speed of the high-pressure pump up to its flow limits result in the increase of power generated by the pelton turbine. The blades of the turbine need to be pitched when the limits of all sub-systems are reached to maximize revenue up to cut-out wind speeds. This optimal operation strategy for both maximum electricity and water production results in the operation of the DOT500 turbine away from the problematic region for all wind speeds. However, the optimization for maximum water production differs from operating the turbine at maximum power performance. The operation/control of the system is dominated by pressure, rather than power.

Sensitivity analysis of critical desalination parameters is performed using the model built to maximize revenue to analyze their effect on system behavior, to aid in the future optimization of the RO system. As the membrane active area, A_m or the permeability coefficient, K_w increases, the rated wind speed of the turbine decreases and thus the blades have to be pitched at lower wind speeds. Both these parameters have no effect on the minimum wind speed at which water production can start. An increase in both A_m and K_w results in the increase in freshwater produced, up to the maximum membrane production limit. As a result, the electricity generated by the system decreases linearly for an increase in A_m and non-linearly for an increase in K_w. The higher the K_w, the lower the system operating pressure to produce the same volumes of water and the system can operate at its maximum limits for a larger range of wind speeds, thus maximizing revenue.

Sensitivity of more sub-system parameters is required to develop clear guidelines for operating the DOT/RO system. The permeability coefficient of the membrane, K_w needs to be precisely known to make a good prediction on the turbine operating settings for optimization. The behavior of the maximum rotational speed of the pelton turbine from the sensitivity analysis results shows that the flow modeling in pelton turbine needs to be further detailed in the next phase for deeper understanding.

7.2 Recommendations for Future Research

- **Wind turbine control strategies:** To maximize the revenue from system operation, a further study into the control of the hydraulic drive train for the optimal mix of water to electricity generation is required, as a function of the wind climate of the location and real time electricity/water prices. Further research on the active pitch control of the turbine is necessary to maintain constant operation at the system limits from rated wind speed up to cut-out wind speeds. Additionally, a control strategy to stop the wind turbine during an emergency due to fluid dynamics needs further research.

- **Model extension:** The current model is used to solve the DOT500 turbine integrated with a simplistic model of the RO with ERD. For future research, the model presented in this thesis can

be improved by adding models for individual membranes in more detail for deeper insights on the performance of the reverse osmosis system. The losses of pressure energy due to pipeline resistance can also be added to the present model.

- **Wind farm design and optimization:** Scaling up the DOT concept from a single turbine to a wind farm is critical for economic feasibility. Hence, further research is necessary to design and simulate a wind farm and optimize it depending on the location. Further research on different control strategies are required to optimize the operation of individual turbines in a wind farm to take into account the wind farm effects and variation of wind within the park. Several case studies can be performed to design the wind farm with either high-pressure flow pipelines from individual turbines or shared pipelines to the RO and pelton systems. In addition, the position of the RO and pelton systems within the farm can be optimized to minimize pressure losses.

- **Financial analysis:** To scale up the DOT concept, especially in developing countries, the production of electricity and water has to be economically more attractive than conventional techniques. This thesis provides a model to calculate the annual revenue generated by the system up to rated wind speeds and also a basic power consumption model. From this model, it is possible to extrapolate the revenue up to cut-out wind speeds by developing a strategy for active pitch control, to maintain operation at the rated wind speed system limit. However, a detailed financial model is required taking into account the capital expenditures and operational expenditures to determine the levelized costs of electricity and water by considering a realistic fixed charge rate.

- **Change in configuration:** A case study for adding an additional high-pressure pump in series with the pelton turbine, operating using the electricity generated by the pelton generator to further produce freshwater, by feeding it to either a separate RO system or the existing RO system can be looked into, for locations where water is more valuable than electricity. Additionally, the possibility of adding another stage of RO desalination to increase recovery from the feed seawater can be investigated.

- **Energy Savings:** Further savings in energy consumption can be achieved by using TFC polyamide membranes with higher water permeability coefficients and selectivities [29]. A detailed RO model can be made using these membrane materials to analyze the effect of reduced hydraulic overpressures required to achieve water flux on the energy consumption of the system.

References

[1]. Competing for Clean Water Has Led to a Crisis. (2020, April 06). Retrieved May 05, 2020, URL https://www.nationalgeographic.com/environment/freshwater/freshwater-crisis/.

[2]. Sabine Lattemann, Maria D Kennedy, Jan C Schippers, and Gary Amy. Global desalination sitution, chapter 2, sustainability science and engineering, volume 2, issn 1871-2711. Technical report, DOI 10.1016/S1871-2711(09)00202-5,2009.

[3]. https://idadesal.org/ * Resource: IDA Water Security Handbook, 2019 – 2020 and GWI DesalData.

[4]. Look to Windward: The Case for Wind Powered Desalination. (2016, Nov 01). URL https://www.waterworld.com/water-utility-management/energy-management/article/16202012/look-to-windward-the-case-for-wind-powered-desalination.

[5]. Diepeveen, N. (2013). On fluid power transmission in offshore wind turbines.

[6]. D. Akgul, M. Çakmakcı, N. Kayaalp, and I. Koyuncu. Cost analysis of seawater desalination with reverse osmosis in turkey. Desalination, 220(1-3):123–131, 2008.

[7]. Membrane Desalination Power Usage Put in Perspective. (n.d.). URL https://amtaorg.com/wp-content/uploads/07_Membrane_Desalination_Power_Usage_Put_In_Perspective.pdf.

[8]. Dormido, H. (2019, August 06). These Countries Are the Most at Risk From a Water Crisis. URL https://www.bloomberg.com/graphics/2019-countries-facing-water-crisis/.

[9]. Smits, R. A. Analysis of a Wind Driven Reverse Osmosis Desalination System. Master's thesis, Delft University of Technology, 2019.

[10]. M. F. Supper. Fluctuating flows on reverse osmosis membranes: An experimental approach for hydraulic drive train wind turbine applications. Master's thesis, Delft University of Technology, 2017.

[11]. MultiMedia LLC. What is reverse osmosis?, 2017. URL https://puretecwater.com/ reverse-osmosis/what-is-reverse-osmosis.

[12]. J.G. Wijmans and R.W. Baker. The solution-diffusion model: a review. Journal of Membrane Science, 107(1-2):1–21, 1995.

[13]. R.W. Baker. Membrane Technology and Applications. Wiley, Chichester, second edition, 2004.

[14]. L. F. Greenlee, D. F. Lawler, B. D. Freeman, B. Marrot, and P. Moulin. Reverse osmosis desalination: water sources, technology, and today's challenges. Water Research, 43(9):2317–48, 2009.

[15]. Spiral Wound Membranes: RO Membranes: SUEZ. URL https://www.suezwatertechnologies.com/products/spiral-wound-membranes.

[16]. M. J. Guirguis, Energy Recovery Devices In Seawater Reverse Osmosis Desalination Plants With Emphasis On Efficiency And Economical Analysis Of Isobaric Versus Centrifugal Devices, (2011).

[17]. Danfoss. Danfoss isave animation,2018. URL https://www.youtube.com/watch?v=J81mcTV7tUw.

[18]. J. van 't Hoff. The function of osmotic pressure in the analogy between solutions and gases. Philosophical Magazine and Journal of Science, Fifth:81–105, 1888.

[19]. Sebastiaan Mulders, Niels Diepeveen, and J. W. Wingerden. Control design, implementation and evaluation for an in-field 500 kw wind turbine with a fixed-displacement hydraulic drivetrain. Wind Energy ScienceDiscussions,pages1–37,052018. doi: 10.5194/wes-2018-35.

[20]. A. R. Bartman, P. D. Christofides, and Y. Cohen. Nonlinear model-based control of an experimental reverse-osmosis water desalination system. Industrial and Engineering Chemistry Research, 48(13): 6126–6136,2009. ISSN0888-5885.

[21]. Yue Wang, Shichang Wang, and Shichang Xu. Experimental Studies on Dynamic Process of Energy Recovery Device for RO Desalination Plants. Desalination,160(2):187–193,2004.

[22]. Robert Bergman. Reverse osmosis and nanofiltration. American Water Works Association,2007.

[23]. Global Wind Atlas. URL https://globalwindatlas.info/.

[24]. Tarievenregeling 2020 - Dunea. (n.d.). URL https://www.dunea.nl/-/media/bestanden/over-dunea/dunea---tarievenregeling-2020.ashx?la=nl-nl&hash=3B131C400562EF8DE96A98E13D8275F3D0ADB391.

[25]. Cost of Living in Aruba. URL https://www.numbeo.com/cost-of-living/country_result.jsp?country=Aruba

[26]. R.B. Bird, W.E. Stewart, and E.N. Lightfoot. Transport Phenomena. John Wiley & Sons, Inc., 7th edition, 1960.

[27]. Richard L Stover. Seawater reverse osmosis with isobaric energy recovery devices. Desalination, 203 (1-3):168–175,2007.

[28]. Energy recovery devices for reverse osmosis applications. (n.d.). Retrieved August 05, 2020, from https://www.danfoss.com/en/products/energy-recovery-devices/hpp/energy-recovery-devices-for-reverse-osmosis-applications/.

[29]. Song, X., Prince, J. A., & Sun, D. D. (n.d.). Relating Water/Solute Permeability Coefficients to the Performance of Thin-Film Nanofiber Composite Forward Osmosis Membrane. Retrieved August 5, 2020.